

Associative learning drives longitudinally-graded presynaptic plasticity of neurotransmitter release along axonal compartments

Aaron Stahl¹, Nathaniel C. Noyes¹, Tamara Boto¹, Miao Jing², Jianzhi Zeng^{3,4,5}, Lanikea B. King¹, Yulong Li^{2,3,4,5}, Ronald L. Davis¹, Seth M. Tomchik^{1*}

¹Department of Neuroscience, The Scripps Research Institute, Scripps Florida, Jupiter, FL 33458, USA

²Chinese Institute for Brain Research, ³State Key Laboratory of Membrane Biology, Peking University School of Life Sciences, ⁴Peking-Tsinghua Center for Life Sciences, ⁵PKU-IDG/McGovern Institute for Brain Research, Beijing, China

*stomchik@scripps.edu

130 Scripps Way #3C1

Jupiter, FL 33458

(561) 228-3496

Keywords: synaptic, bidirectional, potentiation, depression, Cav2, Cacophony, IP3R

1 **Abstract**

2 Anatomical and physiological compartmentalization of neurons is a mechanism to increase the
3 computational capacity of a circuit, and a major question is what role axonal
4 compartmentalization plays. Axonal compartmentalization may enable localized, presynaptic
5 plasticity to alter neuronal output in a flexible, experience-dependent manner. Here we show
6 that olfactory learning generates compartmentalized, bidirectional plasticity of acetylcholine
7 release that varies across the longitudinal compartments of *Drosophila* mushroom body (MB)
8 axons. The directionality of the learning-induced plasticity depends on the valence of the
9 learning event (aversive vs. appetitive), varies linearly across proximal to distal compartments
10 following appetitive conditioning, and correlates with learning-induced changes in downstream
11 mushroom body output neurons (MBONs) that modulate behavioral action selection.
12 Potentiation of acetylcholine release was dependent on the Ca_v2.1 calcium channel subunit
13 *cacophony*. In addition, contrast between the positive conditioned stimulus and other odors
14 required the inositol triphosphate receptor (IP₃R), which was required to maintain responsivity to
15 odors in untrained conditions. Downstream from the mushroom body, a set of MBONs that
16 receive their input from the γ 3 MB compartment were required for normal appetitive learning,
17 suggesting that they represent a key node through which discriminative effects influence
18 appetitive memory and decision-making. These data demonstrate that learning drives valence-
19 correlated, compartmentalized, bidirectional potentiation and depression of synaptic
20 neurotransmitter release, which rely on distinct mechanisms and are distributed across axonal
21 compartments in a learning circuit.

22

23 **Introduction**

24 Neuronal dendrites carry out computations through compartmentalized signaling, while axons
25 have long been considered to carry signals to their terminal fields relatively uniformly following
26 spike initiation. However, anatomical and physiological compartmentalization of axons has
27 been recently documented in neurons from worms through mammals (Boto et al., 2014; Cohn et
28 al., 2015; Hendricks et al., 2012; Rowan et al., 2016). How axonal compartmentalization
29 influences information flow across neuronal circuits and modulates behavioral outcomes is not
30 understood. One functional role for axonal compartmentalization may be to enable localized,
31 presynaptic plasticity to alter output from select axon compartments in a flexible, experience-
32 dependent manner. This would vastly enhance the neuron's flexibility and computational
33 capabilities. One potential function of such compartmentalization would allow independent
34 modulation of axonal segments and/or synaptic release sites by biologically-salient events, such
35 as sensory stimuli that drive learning.

36

37 The anatomical organization of the *Drosophila* mushroom body (MB) makes it an exemplary
38 testbed to study how sensory information is processed during learning and rerouted to alter
39 behavioral outcomes. The MB encodes odor in sparse representations across intrinsic MB
40 neurons, which are arranged in several parallel sets. They project axons in fasciculated
41 bundles into several anatomically-distinct, but spatially adjacent lobes (α/β , α'/β' , and γ)
42 (Crittenden et al., 1998). These bundled axons are longitudinally subdivided into discrete tiled
43 compartments (Aso et al., 2014a). Each compartment receives afferent neuromodulatory input
44 from unique dopaminergic neurons (Aso et al., 2014a; Mao and Davis, 2009), and innervates
45 unique efferent mushroom body output neurons (MBONs) (Aso et al., 2014a). Each set of
46 dopaminergic neurons plays an individual role in learning, with some conveying aversive

47 teaching signals (Schroll et al., 2006; Schwaerzel et al., 2003), others conveying positive
48 teaching signals (Liu et al., 2012; Yamagata et al., 2015), and a third class modulating memory
49 strength without driving valence (Boto et al., 2019). Likewise, each MBON has a unique effect
50 on behavioral approach and avoidance, with some biasing the animal to approach, others
51 biasing the animal to avoidance, and some having no effect (Aso et al., 2014b; Perisse et al.,
52 2016; Placais et al., 2013; Sejourne et al., 2011).

53

54 A major question in learning and memory is how presynaptic plasticity contributes to reweight
55 the flow of sensory signals down each of the downstream “approach” or “avoidance” circuits,
56 altering action selection and memory retrieval. In naïve conditions, *Drosophila* dopaminergic
57 circuits modulate cAMP in a compartmentalized fashion along the MB axons (Boto et al., 2014).
58 This compartmentalized dopaminergic signaling can independently modulate Ca²⁺ responses in
59 each compartment, as well as the responses of the downstream valence-coding MBONs (Cohn
60 et al., 2015). Dopamine-dependent heterosynaptic depression at the MB-MBON synapse
61 modulates learning (Hige et al., 2015a). Therefore, presynaptic plasticity in the MB neurons
62 within each compartment could theoretically drive the changes in MBON responsiveness that
63 guide behavioral learning (Zhang et al., 2019). However, manipulation of the “aversive”
64 protocerebral posterior lateral 1 (PPL1) dopaminergic neurons does not detectably alter Ca²⁺
65 signals in MB neurons (Boto et al., 2019; Hige et al., 2015a). Furthermore, Ca²⁺ responses in
66 MB neurons are uniformly potentiated across compartments with appetitive classical
67 conditioning protocols and unaltered in MB neurons following aversive protocols (Louis et al.,
68 2018). This raises the question of how local, compartmentalized synaptic plasticity in MB
69 neurons drives coherent changes in downstream MBONs to modulate action selection during
70 memory retrieval. Learning/dopamine-induced plasticity has been demonstrated in the
71 downstream MBONs (Berry et al., 2018; Hige et al., 2015a; Hige et al., 2015b; Oswald et al.,

72 2015), with dopamine also acting directly on MBONs (Takemura et al., 2017). Feedforward
73 inhibition among MBONs that drive opposing behavioral outcomes provides a mechanism
74 explaining how valence coding in MBONs could be generated (Perisse et al., 2016). Yet this
75 does not explain the compartmentalized, dopamine-dependent plasticity in MB neurons
76 themselves or the necessity for dopamine receptors and downstream signaling molecules in the
77 intrinsic MB neurons (Kim et al., 2007; McGuire et al., 2003; Zars et al., 2000).

78

79 Here we describe how learning alters the flow of information through the MB via synaptic
80 release of the putative MB neurotransmitter (Barnstedt et al., 2016), using genetically-encoded
81 indicators of synaptic acetylcholine neurotransmission. The data reveal that learning alters the
82 compartmentalized axonal acetylcholine release from *Drosophila* mushroom body (MB) neurons
83 in valence-specific spatiotemporal patterns, via distinct molecular mechanisms, driving
84 behavioral alterations via modulation of specific downstream output neurons.

85

86 **Results**

87 **Associative learning modulates neurotransmitter release in a spatially-distinct manner** 88 **across longitudinal axonal compartments**

89 Synapses within each MB compartment transmit olfactory information from MB neurons to
90 compartment-specific MBONs (Fig. 1A, 5A,B) (Aso et al., 2014a; Tanaka et al., 2008). The
91 MBONs exert distinct and often-opposing effects on behavior, with some innately promoting
92 approach and others promoting avoidance (Aso et al., 2014b; Berry et al., 2018; Ichinose et al.,
93 2015; Oswald et al., 2015; Perisse et al., 2016; Placais et al., 2013; Sayin et al., 2019; Sejourne
94 et al., 2011). Synaptic depression has been observed in the MB-MBON synapses following

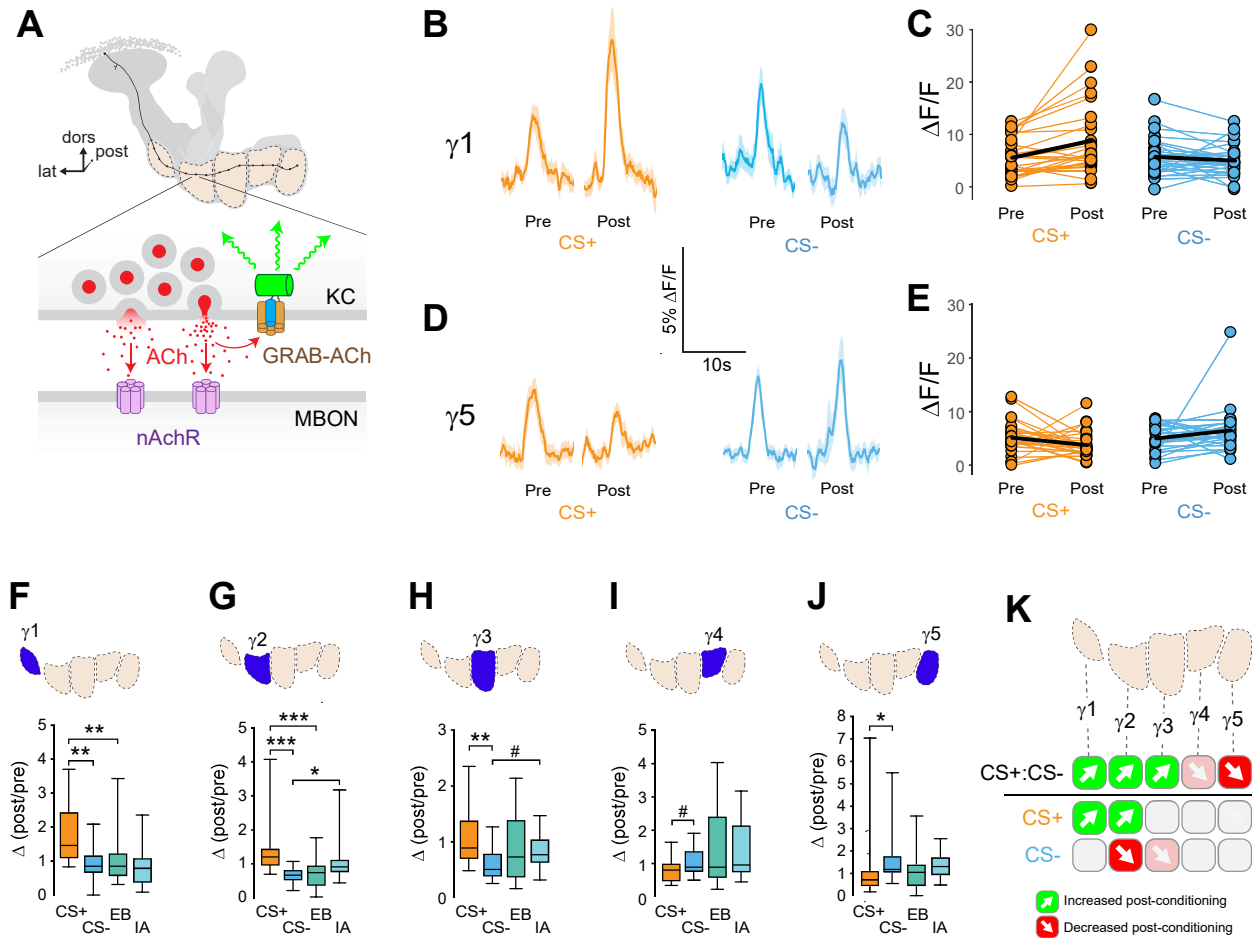


Figure 1. Compartment-specific alterations of ACh release in the MB following appetitive conditioning. **(A)** Diagram of the GRAB-ACh reporter expressed in presynaptic terminals of MB neurons (Kenyon cells: MB). nAChR: nicotinic acetylcholine receptor; dors: dorsal; lat: lateral, post: posterior; MBON: mushroom body output neuron. **(B)** Time series traces showing odor-evoked GRAB-ACh responses pre- and post-conditioning. Responses were imaged to both the CS+ (ethyl butyrate: EB) and CS- (isoamyl acetate: IA) odor in the $\gamma 1$ compartment, and the line and shading represent the mean \pm SEM. **(C)** Quantification of the pre- and post-conditioning responses to the CS+ (EB) and CS- (IA) from the $\gamma 1$ compartment from individual animals ($n = 27$), with the mean graphed as a black line. **(D)** Time series traces imaged from the $\gamma 5$ compartment, graphed as in panel B. **(E)** Quantification of peak responses from the $\gamma 5$ compartment, graphed as in panel C. **(F-J)** Change in odor-evoked responses (Post/pre responses), following conditioning (CS+ and CS-) or odor-only presentation (EB and IA). * $p < 0.01$, ** $p < 0.001$, *** $p < 0.0001$; $n = 27$ (Kruskal-Wallis/Bonferonni). **(F)** $\gamma 1$ compartment. **(G)** $\gamma 2$ compartment. **(H)** $\gamma 3$ compartment. # $p = 0.0169$. **(I)** $\gamma 4$ compartment. # $p = 0.0868$. **(J)** $\gamma 5$ compartment. **(K)** Summary of plasticity in ACh release across γ lobe compartments. Green up arrows indicate increases in the CS+:CS- (1st row) or potentiation of the CS+ response (relative to odor-only controls; 2nd row), while red down arrows indicate decreases in the CS+:CS- (1st row) or depression of the CS- (relative to odor-only controls; 3rd row).

95 pairing of odor with stimulation of PPL1 neurons that are critical for aversive learning (Hige et
96 al., 2015a), suggesting that depression may be a primary mechanism for learning at these
97 synapses (Barnstedt et al., 2016; Cohn et al., 2015; Handler et al., 2019; Oswald et al., 2015;
98 Perisse et al., 2016; Sejourne et al., 2011). One synapse downstream, some MBONs exhibit
99 bidirectional responses to conditioning, though the major described mechanism involves a sign
100 change that occurs postsynaptic to the MBs (polysynaptic feedforward inhibition) (Owald et al.,
101 2015; Perisse et al., 2016). To test for the presence, directionality, and variation of presynaptic
102 plasticity across MB axonal compartments, we expressed a synaptic ACh sensor to monitor
103 neurotransmitter release from MB neurons *in vivo* (Zhang et al., 2019). The genetically-
104 encoded ACh reporter, GPCR-Activation–Based-ACh sensor (GRAB-ACh) (Fig. 1A) (Jing et al.,
105 2019; Jing et al., 2018; Zhang et al., 2019), was expressed in MB neurons using the 238Y-Gal4
106 driver. Appetitive conditioning was carried out, monitoring ACh release from the γ lobe
107 compartments evoked by the CS+ and CS- before and after pairing odor with sucrose (Fig. S1).
108 Responses were compared to those in odor-only control cohorts to determine whether any
109 learning-induced changes resulted from potentiation or depression. We quantified several
110 parameters (Fig. S1), including how the responses changed after conditioning (the within-
111 treatment post/pre). In addition, we compared the CS+ and CS- responses after conditioning
112 (CS:CS-), which mimics the putative comparison the animal makes during associative memory
113 retrieval. Finally, we compared the change in CS+ and CS-, $\Delta(\text{post/pre})$, to their respective
114 odor-only controls to quantify whether they were potentiated or depressed by conditioning,
115 accounting for any sensory adaptation (Figs. 1 F-J, S2).

116

117 Appetitive conditioning produced plasticity in ACh release that varied across the axonal
118 compartments of the MB γ lobe in several key ways (Fig. 1). Conditioning significantly

119 increased CS+ responses relative to the CS- responses (\uparrow CS+:CS-) in the three most proximal γ
120 lobe compartments: γ 1, γ 2, and γ 3 (Figs. 1 B,C,F-H; S2). In each of these compartments, this
121 was due to different underlying mechanisms. In the γ 1 compartment, the CS+ response was
122 potentiated; i.e., following appetitive conditioning, the Δ (post/pre) CS+ response was larger than
123 the ethyl butyrate (EB) odor-only control, while the CS- did not significantly differ from the
124 isoamyl acetate (IA) odor-only control (Figs. 1F, S2). In the γ 2 compartment, both the CS+ was
125 potentiated and the CS- depressed relative to the odor-only controls (Figs. 1G, S2). Finally, in
126 the γ 3 compartment, neither was significantly altered relative to odor-only controls at the
127 Bonferroni-corrected $\alpha=0.01$ level, but there was a strong trend toward depression with the CS-
128 group (Figs. 1H, S2). Thus, there was a spatial gradient of CS+ potentiation in γ 1, shifting from
129 CS+ potentiation in γ 1 toward CS- depression in γ 3, with the spatially-intermediate γ 2 exhibiting
130 both. This gradient of CS+:CS- plasticity suggests that both the CS+ and CS- contribute to
131 learning by modulating MB output.

132

133 In the distal γ 4- γ 5 compartments, appetitive conditioning produced plasticity in the opposite
134 direction to that in the proximal γ compartments. In these compartments, the CS+ response
135 was reduced relative to the CS- (\downarrow CS+:CS-) (Figs. 1D, E, I-J, S2). This effect was significant in
136 the γ 5 compartment (Fig. 1J), while γ 4 exhibited a trend in the same direction (Fig. 1I). In these
137 compartments, the effect could not be unambiguously assigned to CS+ depression, though
138 there was no evidence of CS- potentiation (Figs. 1 I,J, S2). Overall, appetitive conditioning
139 produced net enhancement of CS+ responsivity in γ 1- γ 3 compartments, which was derived from
140 a proximal-to-distal gradient of CS+ potentiation to CS- depression, and net reduction of CS+
141 responsivity in γ 4- γ 5 (Fig. 1K). Thus, the plasticity was bidirectional between the proximal and
142 distal axonal compartments. This likely contributes to approach behavior by simultaneously

143 enhancing the conditioned odor-evoked activation of downstream “approach” circuits and
144 inhibition of “avoidance” MBON circuits.

145

146 **Conditioning with opposing valence stimuli generates bidirectional presynaptic plasticity**
147 **within axonal compartments**

148 The above data suggested that appetitive conditioning produced synaptic potentiation in the
149 proximal γ lobe compartments. Yet synaptic depression is the main described plasticity
150 mechanism at the MB-MBON synapses following olfactory conditioning (Barnstedt et al., 2016;
151 Modi et al., 2020; Oswald et al., 2015; Perisse et al., 2016; Sejourne et al., 2011; Zhang and
152 Roman, 2013; Zhang et al., 2019). In the γ_1 compartment, where it has been examined in
153 detail with electrophysiology, aversive reinforcement substitution produces synaptic depression
154 (Hige et al., 2015a). Since many of these studies involved aversive conditioning, we reasoned
155 that appetitive and aversive conditioning may produce bidirectional plasticity, with the
156 sign/directionality matching postsynaptic MBON valence. To test this, we examined whether
157 aversive conditioning produced the opposite effect in the same compartments as appetitive
158 conditioning had. ACh release from MB neurons was imaged with GRAB-ACh and flies were
159 trained with an aversive odor-shock conditioning protocol (Fig. 2A). In these experiments, we
160 focused on the γ_2 - γ_5 compartments, as the fly was mounted at a higher angle, making the
161 GRAB-ACh signal difficult to simultaneously visualize from γ_1 along with that of the other
162 compartments. Following aversive conditioning, there was a reduction in the CS+ response
163 relative to the CS- (\downarrow CS+:CS-) in the γ_2 and γ_3 compartments (Fig. 2 C-H). This was due to
164 depression in the CS+ response, as the post-conditioning CS+ response was significantly
165 smaller than odor-only controls. The γ_4 and γ_5 compartments exhibited no significant change in
166 ACh release (Fig 2 I-J). When compared to appetitive conditioning, aversive stimuli produced

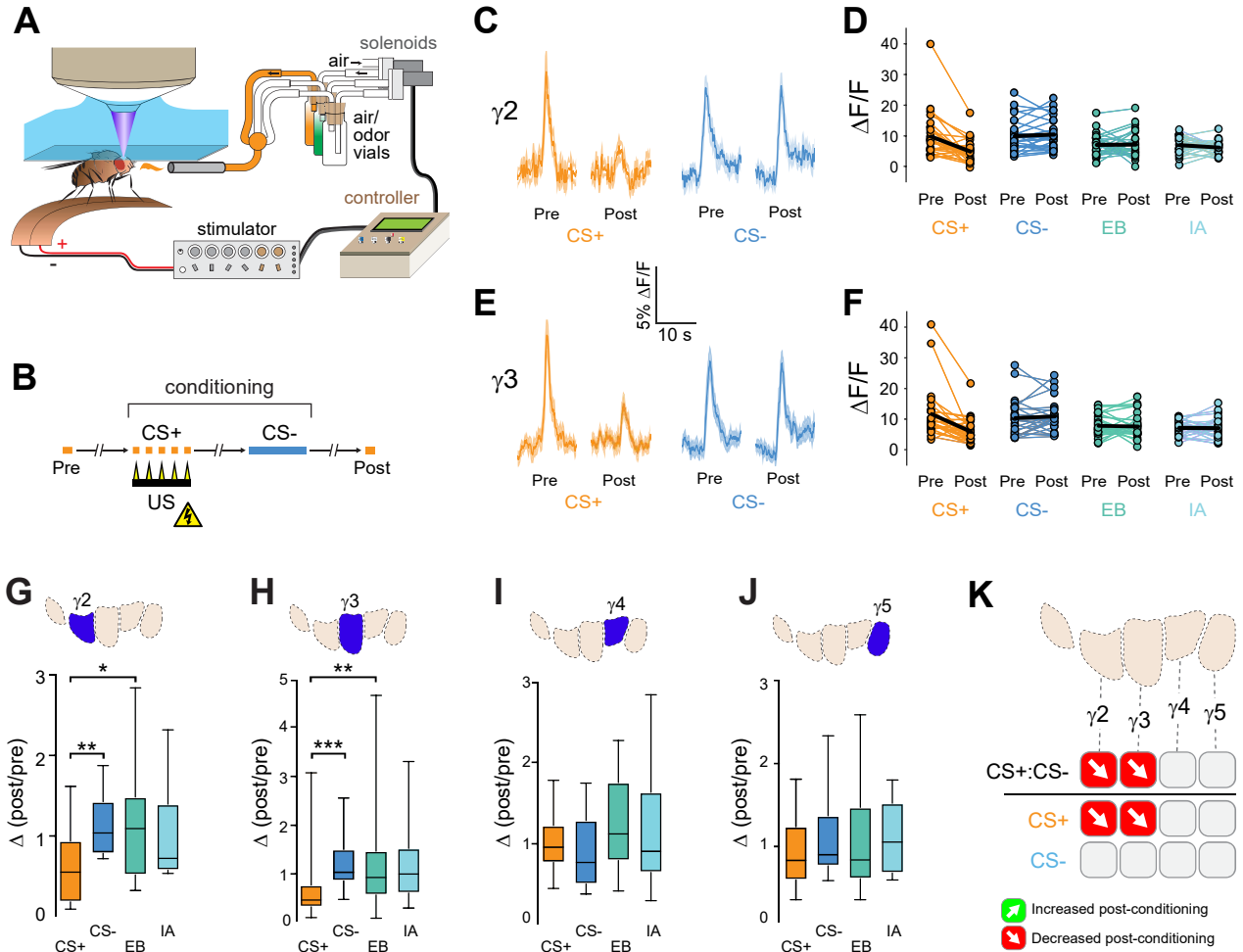


Figure 2. Compartment-specific alterations of ACh release in the MB following aversive conditioning. **(A)** Diagram of the aversive conditioning apparatus. **(B)** Aversive conditioning experimental protocol, pairing an odor (the CS+) with an electric shock unconditioned stimulus (US) (6 shocks, 60V). A second odor, the CS- was presented 5 min after pairing the CS+ and US. One odor was imaged before (Pre) and after (Post) conditioning per animal (CS+ diagrammed here). **(C)** Time series traces showing odor-evoked GRAB-ACh responses pre- and post-conditioning. Responses were imaged to both the CS+ (ethyl butyrate: EB) and CS- (isoamyl acetate: IA) odor in the γ_2 compartment, and the line and shading represent the mean \pm SEM. **(D)** Quantification of the peak pre- and post-conditioning responses to the CS+ (EB) and CS- (IA) from the γ_2 compartment from individual animals ($n = 27$), with the mean graphed as a black line. **(E)** Time series traces imaged from the γ_3 compartment, graphed as in panel B. **(F)** Quantification of peak responses from the γ_3 compartment, graphed as in panel C. **(G-J)** Change in odor-evoked responses (Post/pre responses), following conditioning (CS+ and CS-) or odor-only presentation (EB and IA). * $p < 0.01$, ** $p < 0.001$, *** $p < 0.0001$; $n = 27$ (Kruskal-Wallis/Bonferonni). **(G)** γ_2 compartment. **(H)** γ_3 compartment. **(I)** γ_4 compartment. **(J)** γ_5 compartment. **(K)** Summary of plasticity in ACh release across γ lobe compartments. Red down arrows indicate decreases in the CS+:CS- (1st row) or depression of the CS+ (relative to odor-only controls; 2nd row).

167 plasticity that created a sign flip in the $\gamma 2$ and $\gamma 3$ compartments (Figs. 1K, 2K). Thus, appetitive
168 and aversive conditioning produced bidirectional plasticity across multiple compartments, which
169 was due to localized plasticity within MB γ lobe. The aversive conditioning-induced depression
170 likely represents a presynaptic contribution to learning-induced changes in odor responsivity
171 among postsynaptic MBONs (Berry et al., 2018; Hige et al., 2015a; Oswald et al., 2015; Zhang et
172 al., 2019).

173

174 **Presynaptic potentiation relies on the *cacophony* $Ca_v2.1$ Ca^{2+} channel**

175 Associative learning alters Ca^{2+} transients in MB γ neurons (Louis et al., 2018), which could
176 influence neurotransmitter release. Major sources of stimulus-evoked intracellular Ca^{2+} include
177 influx through voltage-sensitive Ca_v2 channels, which are involved in presynaptic short-term
178 and homeostatic plasticity (Frank et al., 2006; Inchauspe et al., 2004; Ishikawa et al., 2005;
179 Muller and Davis, 2012). To probe the mechanisms of Ca^{2+} -dependent molecular mechanisms
180 underlying presynaptic plasticity, we first knocked down the α subunit of the Ca_v2 Ca^{2+} channel
181 encoded by *cacophony* (*Cac*), in the mushroom body. *Cac* was knocked down conditionally in
182 adult MBs with RNAi using the R13F02-Gal4 driver, combined with the ubiquitous temperature-
183 sensitive tub-Gal80^{ts} repressor (McGuire et al., 2003) to circumvent any potential for
184 developmental effects (Fig. 3A). RNAi expression was induced four days prior to the
185 experiment, and ACh release from MB neurons was imaged with GRAB-ACh (Jing et al., 2018;
186 Zhang et al., 2019). Control flies (containing R13F02-Gal4, UAS-GRAB-ACh, and tub-Gal80^{ts},
187 but lacking a UAS-RNAi) exhibited plasticity across the γ lobe in the same spatial patterns as
188 previously observed: there was an increase in relative CS+ responses in the $\gamma 1$ - $\gamma 3$
189 compartments, and a trend toward a CS+ decrease in $\gamma 5$ (Fig. 3 C,E,F, S4). When *Cac* was
190 knocked down conditionally, odor-evoked ACh release was still observed, demonstrating that

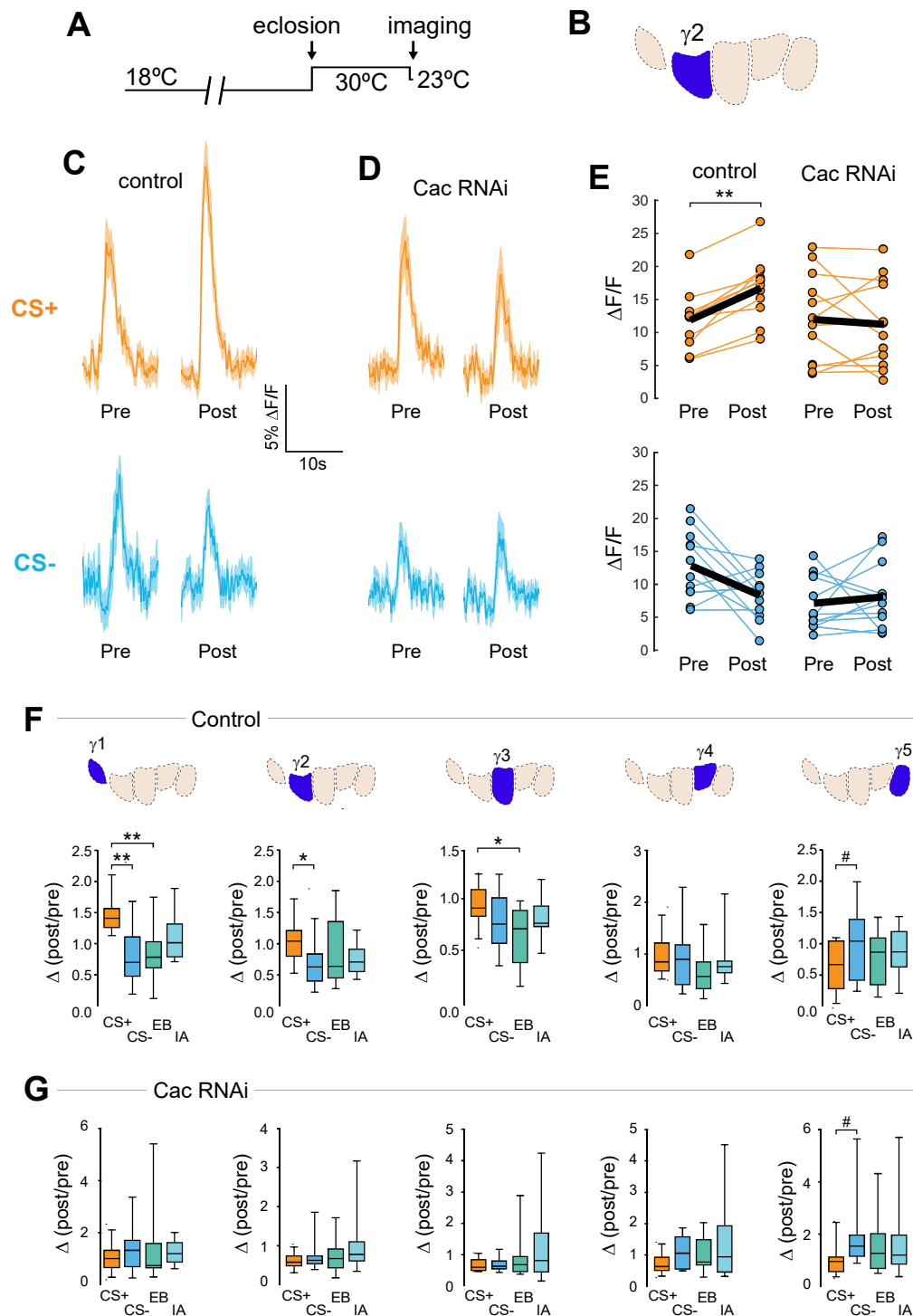


Figure 3. Conditional knockdown of the Ca_v2 channel *Cac* impairs potentiation of ACh release from the MB following appetitive conditioning. **(A)** Diagram of the temperature shifts employed for conditional knockdown of *Cac* with *tub-Gal80ts*. **(B)** Diagram of the MB compartments, highlighting the $\gamma 2$ compartment that was imaged for the data shown in panels C-E. **(C)** Pre- and post-conditioning CS+ (orange; top) and CS- (blue; bottom) odor-evoked ACh release from the $\gamma 1$ compartment before and after appetitive conditioning, imaged in control animals (*w*;UAS-GRAB-ACh/+; R13F02-Gal4/UAS-*tub-Gal80ts*). Time series trace with line and shading representing mean \pm S.E.M. **(D)** CS+ and CS- odor-evoked ACh release from the $\gamma 1$ compartment in animals with conditional knockdown of *Cac* (*w*;UAS-GRAB-ACh/UAS-*Cac*-RNAi;R13F02-Gal4/UAS-*tub-Gal80ts*). **(E)** Pre- and post-conditioning $\Delta F/F$ CS+ and CS- responses in control and *Cac* knockdown animals. **(F)** Change in ACh release (post/pre response) following appetitive conditioning (CS+ and CS-) and odor-only presentation (EB: ethyl butyrate; IA: isoamyl acetate) in control animals across the five MB γ lobe compartments: $\gamma 1$ - $\gamma 5$ (left to right). **(G)** Change in ACh release across the five MB compartments in animals with conditional knockdown of *Cac*. ** $p < 0.01$, * $p < 0.05$; # $p < 0.07$; $n = 12$.

191 synaptic exocytosis remained intact. Yet the CS+ potentiation was lost across the γ 1- γ 3
192 compartments (Fig. 3 D,G, S4). This demonstrates that potentiation of ACh release to the
193 trained odor – induced by learning – is dependent on the presynaptic $\text{Ca}_v2.1$ channel *Cac*.

194

195 Data from the appetitive conditioning experiments suggested that potentiation of the CS+
196 response was dependent on *Cac*. Interestingly, the trend toward CS+ depression in the most
197 distal γ 5 compartment remained intact when *Cac* was knocked down (Fig. 3). This suggests
198 that presynaptic potentiation, but not depression, requires the voltage-sensitive Ca_v2 Ca^{2+}
199 channel *cacophony* across the MB compartments. To further examine whether depression of
200 the CS+ was affected, we turned to aversive conditioning, which generates robust CS+
201 depression in the proximal γ compartments (Fig. 2). Control flies for conditional knockdown
202 experiments exhibited similar CS+ depression in the proximal γ 2,3 lobes. Knock down of *Cac*
203 did not appreciably impair depression of CS+ responses. There was a significant depression in
204 γ 2, both in terms of CS+:CS- and CS+ relative to odor-only controls (Figs. 4, S5). In γ 1, there
205 was a trend toward a decrease in the CS+:CS- ratio that matched the controls (Fig. S5). In γ 3,
206 the difference between the CS+ and CS- (or odor-only control) did not reach significance, but
207 there was a trend in the same direction as the controls (Fig. S5). Overall, these data
208 demonstrate that *Cac* is not required for learning-induced depression of ACh release.

209

210 **Post-conditioning odor contrast and maintenance of odor responses are dependent on** 211 **IP_3 signaling**

212 Ca^{2+} release from the endoplasmic reticulum (ER) is a major source of stimulus-evoked Ca^{2+} in
213 neurons, including MB neurons, and modulates various forms of synaptic/homeostatic plasticity

214 (Handler et al., 2019; James et al., 2019; Taufiq et al., 2005). Therefore, we reasoned that
215 inositol triphosphate receptor (IP₃R) mediated Ca²⁺ release may contribute to presynaptic
216 plasticity across MB compartments. To test this, we conditionally knocked down the IP₃R in the
217 adult MB with RNAi. GRAB-ACh was expressed in the MB (as above) while conditionally
218 knocking down IP₃R (Fig. 4, S5). For these experiments, flies were aversively conditioned (IP₃R
219 knockdown impairs feeding under the microscope, precluding appetitive conditioning).
220 Knockdown of IP₃R eliminated the post-conditioning contrast between the CS+ and CS- (i.e.,
221 the difference between the CS+ and CS-) (Fig. 4, S5). This was due to increased adaptation to
222 the odors (reduction in post-conditioning odor responses). This occurred in the CS- and both
223 odor-only control groups, bringing them down to a similar level to the level of the CS+ group
224 (Fig. 4 C-E). Thus, in normal conditions, release of Ca²⁺ from the ER via IP₃R is necessary to
225 maintain odor responsivity upon repeated odor presentations. Loss of IP₃R renders the MB
226 neurons more susceptible to adaptation, reducing the contrast between the CS+ – which
227 exhibits depression following aversive learning – and the other odor(s).

228

229 **Compartmentalized plasticity propagates into downstream mushroom body output** 230 **neurons**

231 Since ACh release from each compartment provides input to unique postsynaptic mushroom
232 body output neurons, the presynaptic plasticity observed in each compartment should be
233 mirrored in the respective postsynaptic MBON(s) innervating that compartment. To test this, we
234 imaged Ca²⁺ responses in MBONs with GCaMP and examined the effect of appetitive
235 conditioning. Four sets MBONs were tested, each innervating and receiving cholinergic input
236 from a distinct MB γ lobe compartment: γ_1 pedc> α/β , $\gamma_2\alpha'1$, $\gamma_3/\gamma_3\beta'1$, and $\gamma_5\beta'2a$ (Fig. 5A).
237 Within the γ lobe, these neurons innervate the γ_1 , γ_2 , γ_3 , and γ_5 compartments, respectively

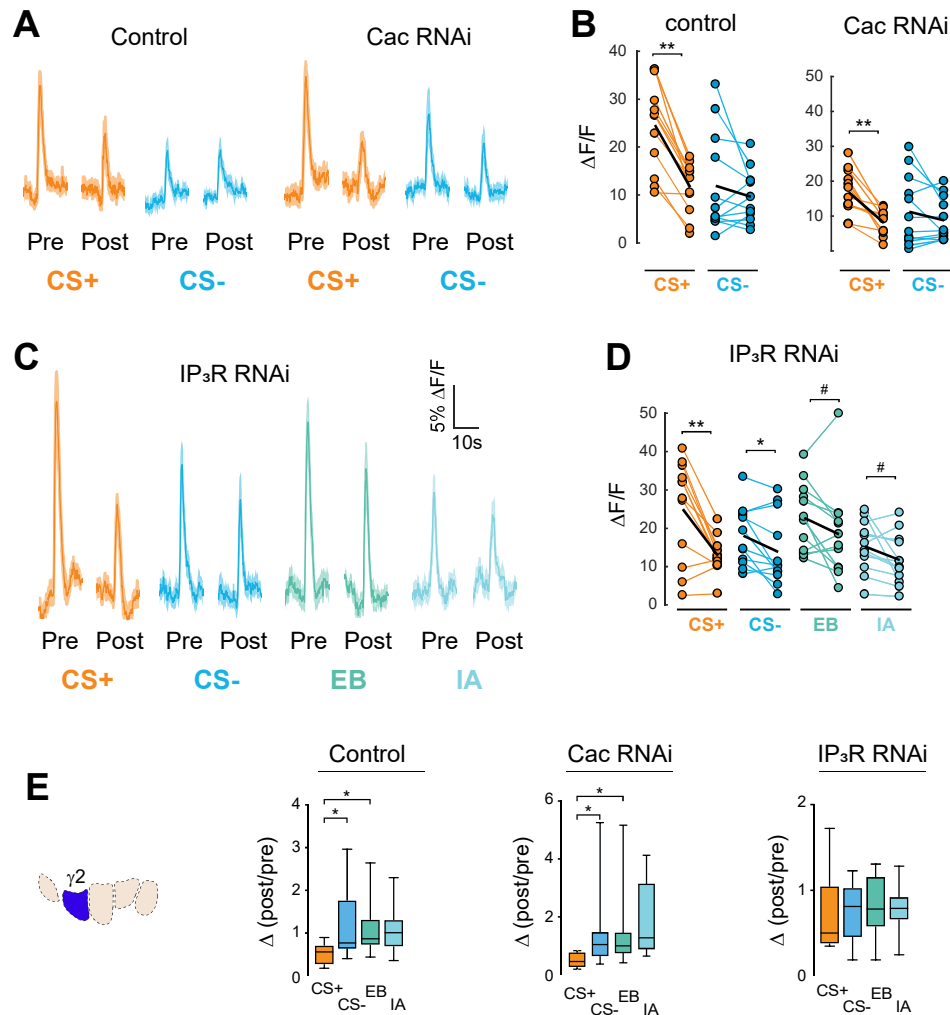


Figure 4. Cac and IP₃R exert distinct effects on synaptic plasticity and maintenance of olfactory responses following aversive conditioning. **(A)** Pre- and post-conditioning CS+ and CS- odor-evoked ACh release in control and Cac RNAi flies. Time series trace with line and shading representing mean \pm S.E.M. **(B)** Pre- and post-conditioning $\Delta F/F$ CS+ and CS- responses in control and Cac knockdown animals. Each thin line connects the pre- (left) and post-conditioning response (right) for one animal. The thick black line represents the mean. **(C)** ACh release in IP₃R knockdown animals for trained odors (CS+ and CS-) as well as the respective odor-only controls (ethyl butyrate [EB] and isoamyl acetate [IA]). **(D)** $\Delta F/F$ responses in IP₃R knockdown flies. **(E)** Change in ACh release (post/pre response) following aversive conditioning (CS+ and CS-) and odor-only presentation (EB and IA) in controls, as well as flies with conditional Cac and IP₃R knockdown.

238 (Fig. 5 B-F). The $\gamma 1_{pedc>\alpha/\beta}$ MBON exhibited a significant elevation of the CS+ response
239 relative to the CS- ($\uparrow CS+:CS-$) (Fig. 5H). This was due to a potentiation of the CS+ response,
240 as the post-conditioning CS+ response was significantly larger than the corresponding odor-only
241 control. The $\gamma 2_{\alpha'1}$ MBON also exhibited an increase in the CS+:CS- ratio following conditioning
242 (Fig. 5I). In this neuron, the plasticity could not be unambiguously attributed to purely CS+
243 potentiation or CS- depression. The $\gamma 3/\gamma 3\beta'1$ MBONs exhibited an increase in the CS+:CS- that
244 was due to potentiation of the CS+ response (Fig. 5J). Note that these neurons are not parsed
245 with available drivers and were imaged as a pair. Presynaptically, the $\gamma 3$ compartment exhibited
246 a depression in the CS- response, suggesting that the potentiation in the MBON CS+ response
247 may emanate either from the $\beta'1$ inputs or modulation via polysynaptic circuit interactions.
248 Finally, appetitive conditioning produced plasticity in the opposite direction in the $\gamma 5\beta'2a$ MBON;
249 this neuron exhibited a decrease in the CS+ response relative to the CS- ($\downarrow CS+:CS-$) (Fig. 5K).
250 In each case, the directionality of the plasticity (CS+:CS-) matched that observed in ACh
251 responses in the presynaptic compartment. Thus, compartmentalized, presynaptic plasticity in
252 neurotransmitter release from the MB compartments likely plays a role in modulating the MBON
253 responses following learning.

254

255 **Isolation of timing effects reveals CS- specific depression in the $\gamma 3$ compartment**

256 Synaptic depression in ACh release in the $\gamma 2$ and $\gamma 3$ compartments following appetitive
257 conditioning was unique in that, in wild-type animals, it involved plasticity to the CS- (Figs. 2
258 G,H, S3). This raised the question of whether the simple act of presenting an odor 30 seconds
259 after the offset of US pairing – the time at which the CS- is presented in the conditioning
260 paradigm – is sufficient to alter ACh release. To test this, we compared the results from the
261 discriminative CS+/CS- imaging assay (Figs. 2, S3) with a single-odor paradigm (Fig. 6A). Flies

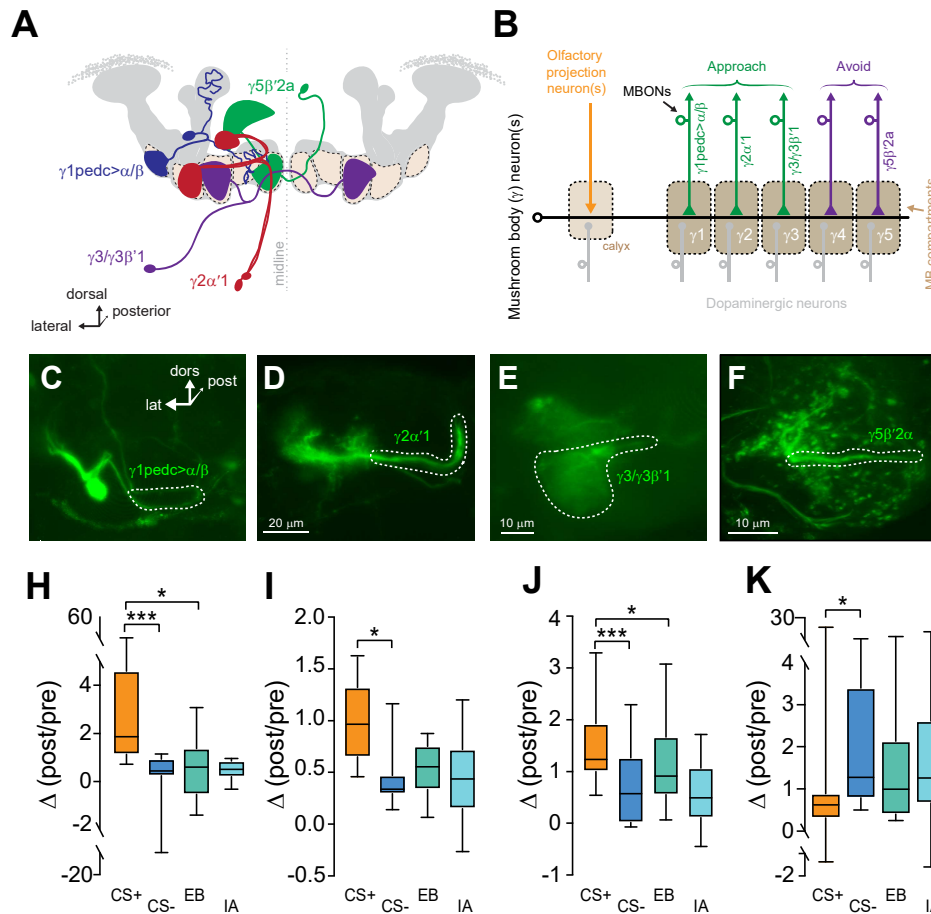


Figure 5. Plasticity in MBON Ca^{2+} responses mirrors compartmental plasticity in the MB neurons. **(A)** Diagram of MBONs innervating specific γ lobe compartments, viewed from a frontal plane. Each MBON is bilaterally paired, though only one is drawn here for visual clarity. **(B)** Circuit diagram of the dopaminergic neurons and MBONs in each compartment, as well as the putative valence associated with each compartment/MBON. **(C-F)** Diagrams of the $\gamma 1pedc>\alpha/\beta$, $\gamma 2\alpha'1$, $\gamma 3$, and $\gamma 5\beta'2\alpha$ MBONs, respectively, drawn unilaterally in isolation. **(G-J)** Representative confocal images of the $\gamma 1pedc>\alpha/\beta$, $\gamma 2\alpha'1$, $\gamma 3$, and $\gamma 5\beta'2\alpha$ MBONs, respectively. The region of interest circumscribed for quantification (neuropil or an efferent neurite) is drawn with a dotted white line. lat: lateral, dors: dorsal, post: posterior. **(K-N)** Change in odor-evoked responses (Post/pre responses), following conditioning (CS+ and CS-). *** $p < 0.001$, * $p < 0.01$; $n = 12$ (Kruskal-Wallis/Bonferroni).

262 expressing GRAB-ACh in the MB via the 238Y-Gal4 driver were presented with an odor and
263 sucrose, in a similar manner to the standard discriminative appetitive conditioning protocol,
264 except that the CS+, CS-, or US was omitted (Fig. 6A, S6). We compared the change in
265 responses to that odor across the three protocols in all five compartments (Fig. 6C, S3). This
266 revealed several major facets of plasticity in ACh release following appetitive conditioning. First,
267 discriminative training is necessary for the potentiation in $\gamma 1$ and $\gamma 2$, which was lost in single-
268 odor CS/US training (protocol #1) (Fig. 6A,C, S6). In addition, when omitting the CS+, only the
269 $\gamma 3$ compartment revealed significant timing effects (Fig. 6 B,C, S6); presenting sucrose prior to
270 presentation of an odor in the normal CS- time slot (protocol #2) resulted in a significantly
271 smaller response than CS/US pairing, as well as a trend toward depression relative to the odor-
272 only group. Therefore, the backward temporal contingency of the odor and sucrose
273 presentation likely underlies the depression of odor-evoked responses in the $\gamma 3$ region observed
274 with discriminative CS+/CS- learning (Fig. 2H). Overall, these data demonstrate that the $\gamma 3$
275 compartment is particularly important for the temporal comparison of the CS+ and CS-, which is
276 critical for discriminative learning (a possibility we explore further below).

277

278 **Synaptic activity from the $\gamma 3$ -innervating MBONs mediate appetitive learning**

279 The unique role of the $\gamma 2$ and $\gamma 3$ compartments in encoding CS- plasticity led us to question the
280 behavioral roles of the MBONs that receive input from these compartments (Figs. 1, 6A-C).
281 With the exception of the $\gamma 1pedc>\alpha/\beta$ (Perisse et al., 2016), the involvement of these MBONs in
282 appetitive memory is unclear. To test whether the MBONs innervating the $\gamma 2$ and $\gamma 3$
283 compartments mediate appetitive memory, we carried out behavioral appetitive classical
284 conditioning, blocking synaptic transmission from MBONs with *Shibire^{ts}* (*Shi^{ts}*) (McGuire et al.,
285 2001) (Fig. 6 D,E). Blocking the $\gamma 2\alpha'1$ MBON did not significantly impair performance in

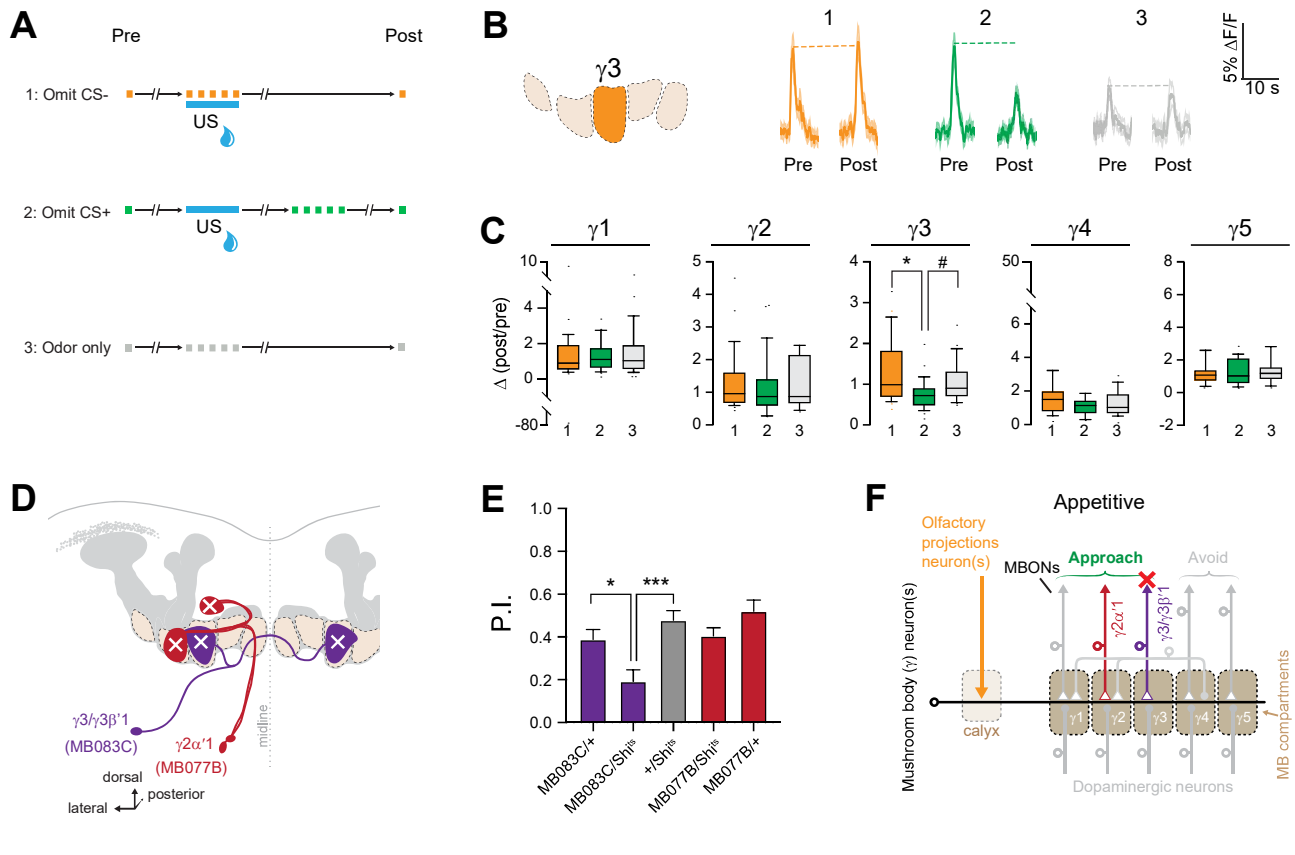


Figure 6. MB $\gamma 3$ plasticity encodes appetitive timing (CS-) effects, and output neurons from this region are necessary for appetitive learning. **(A)** Diagram of the training paradigms utilized for ACh imaging experiments. **(B)** Time series traces showing odor-evoked GRAB-ACh responses from the $\gamma 3$ compartment with all three protocols. **(C)** Quantification of the odor-evoked post/pre responses from each γ lobe compartment. * $p < 0.01$, # $p = 0.016$; $n = 27$ (Kruskal-Wallis/Bonferroni). **(D)** Anatomical Diagram of the $\gamma 2\alpha'1$ (MB077B-Gal4) and $\gamma 3/\gamma 3\beta'1$ (MB083C-Gal4) MBONs. **(E)** Behavioral appetitive conditioning in flies, silencing either $\gamma 2\alpha'1$ or $\gamma 3/\gamma 3\beta'1$ MBONs with Shibirets (Shits), compared to heterozygous Gal4/+ and UAS/+ controls. P.I.: Performance Index. * $p < 0.05$, *** $p < 0.0005$ (ANOVA/Sidak); $n = 16$. **(F)** Circuit diagram of the output of the $\gamma 2\alpha'1$ and $\gamma 3/\gamma 3\beta'1$ MBONs.

286 appetitive conditioning. Therefore, while activation of the $\gamma 2\alpha'1$ MBON drives approach
287 behavior (Aso et al., 2014b) and the neuron is necessary for aversive memory (Berry et al.,
288 2018), it is not crucial for appetitive learning in the otherwise intact nervous system. In contrast,
289 blocking synaptic transmission from the $\gamma 3/\gamma 3\beta'1$ MBONs significantly impaired appetitive
290 conditioning performance (Fig. 6E). This demonstrates that the output of the $\gamma 3/\gamma 3\beta'1$ MBONs is
291 necessary for normal appetitive short-term memory (Fig. 6F). These neurons convey the output
292 of the MB $\gamma 3$ compartment to the crepine and superior medial protocerebrum (where they
293 innervate interneurons that project to the fan-shaped body and lateral accessory lobe further
294 downstream), as well as provide direct contralateral MB feedback and form polysynaptic
295 feedback loops via MB-innervating PAM dopaminergic neurons and other MBONs (Scaplen et
296 al., 2021; Xu et al., 2020). These multi-layered connections provide several routes through
297 which they could modulate behavioral output following learning. Overall, the present data
298 suggest that the $\gamma 3/\gamma 3\beta'1$ MBONs receive input from an MB compartment with unique
299 physiology, and represent a key node through which discriminative effects influence appetitive
300 memory and decision-making.

301

302 **Discussion**

303 Compartmentalized plasticity in neurotransmitter release expands the potential computational
304 capacity of learning circuits. It allows a set of odor-coding mushroom body neurons to bifurcate
305 their output to different downstream approach- and avoidance-driving downstream output
306 neurons, independently modulating the synaptic connections to alter action selection based on
307 the conditioned value of olfactory stimuli. The MB modifies the encoded value of olfactory
308 stimuli through bidirectional plasticity in odor responses, which are compartment-specific along
309 the axons. The CS+ and CS- drive unique patterns of plasticity in each compartment,

310 demonstrating that olfactory stimuli are reweighted differently across compartments following
311 learning, depending on the temporal associations of the stimuli. Different molecular
312 mechanisms regulate the potentiation of trained odor responses (Ca_v2/Cac) and maintenance
313 of responsivity over time (IP_3R). Finally, one set of γ output neurons, the $\gamma3/\gamma3\beta'1$ MBONs, is
314 particularly important for appetitive short-term memory.

315

316 The present data reveal learning-induced, bidirectional plasticity of ACh release in the MB
317 neurons following conditioning with naturalistic stimuli *in vivo*, which was compartmentally-
318 localized and coherent with the innate valence of the MBON innervating the compartment.
319 Notably, the $\gamma2$ and $\gamma3$ compartments, which relay information to approach-promoting MBONs
320 (Aso et al., 2014b), exhibited enhanced CS+:CS- responses to appetitive conditioning, and
321 conversely reduced CS+:CS- following aversive conditioning. This was observed within 5
322 minutes of conditioning, a time point consistent with short-term memory in behavioral assays.
323 Previous studies have described short-term, heterosynaptic depression in the $\gamma1pedc$ MBON
324 following reinforcement substitution via PPL1 dopaminergic neuron stimulation (Hige et al.,
325 2015a) and changes in odor-evoked Ca^{2+} responses following olfactory classical conditioning
326 (Perisse et al., 2016). Aversive conditioning has also been shown to decrease neurotransmitter
327 release from the MB neurons (Zhang and Roman, 2013; Zhang et al., 2019). Indirect evidence,
328 via Ca^{2+} imaging in presynaptic MB neurons, has suggested that increases in presynaptic
329 neurotransmission could be associated with learning. Specifically, reinforcement substitution by
330 pairing odor with stimulation of appetitive PAM dopaminergic neurons potentiates odor-evoked
331 cytosolic Ca^{2+} transients across the MB (Boto et al., 2014). In addition, appetitive conditioning
332 with naturalistic odor + sucrose pairing increases odor-evoked cytosolic Ca^{2+} transients in MB
333 neurons (Louis et al., 2018). However, all MB compartments exhibit plasticity with uniform

334 directionality; short-term aversive conditioning produces no detectable change and appetitive
335 conditioning uniformly elevates odor-evoked responses across the $\gamma 1$ - $\gamma 5$ compartments. Thus,
336 this effect is not selective for subcellular MB compartments that connect to the “aversive” or
337 “appetitive” MBONs. More compartmentalized effects have been observed with other
338 manipulations – presentation of sucrose alters synaptically-localized Ca^{2+} transients in a
339 compartmentalized manner (Cohn et al., 2015), as does stimulation of $\gamma 4$ -innervating
340 dopaminergic circuits (Handler et al., 2019).

341

342 This study revealed two major mechanisms regulating the spatial patterns of compartmentalized
343 plasticity across the MB compartments: a *Cac*-dependent CS+ potentiation and an IP_3R -
344 dependent maintenance of sensory responses. This suggests that different sources of
345 intracellular Ca^{2+} play different roles in regulating MB synaptic responses. *Cac* is the pore-
346 forming subunit of the voltage-sensitive, presynaptic Ca_v2 Ca^{2+} channel in *Drosophila*. Ca_v2
347 channels regulate several forms of synaptic plasticity, including paired-pulse facilitation,
348 homeostatic plasticity, and long-term potentiation (Frank et al., 2006; Inchauspe et al., 2004;
349 Nanou et al., 2016). Our data suggests that these channels regulate the spatial patterns of
350 learning-induced plasticity in the MB unidirectionally, with *Cac* underlying potentiation but not
351 depression. Ca_v2 channel activity is modulated by presynaptic calcium and G protein-coupled
352 receptor activity (Zamponi and Currie, 2013), and channel localization in the active zone
353 dynamically regulates synaptic strength (Gratz et al., 2019; Lubbert et al., 2019). These
354 mechanisms may play a role in increasing CS+ responses following appetitive conditioning, as
355 activity in MB neurons results in increased intracellular Ca^{2+} and dopaminergic neurons
356 innervating the MB activate receptors that are important for memory formation (Boto et al.,
357 2014; Cohn et al., 2015; Gervasi et al., 2010; Kim et al., 2007; Schwaerzel et al., 2003; Tomchik
358 and Davis, 2009). Baseline stimulus-evoked neurotransmitter release in *Cac* knockdown was

359 maintained, likely mediated by either residual Cac expression or compensation by other
360 intracellular Ca²⁺ channels/sources. In contrast to potentiation, IP₃R was necessary to maintain
361 normal odor responsivity when odors were presented on multiple trials (i.e., across pre/post
362 odor presentations). This is consistent with the role of IP₃R in maintenance of presynaptic
363 homeostatic potentiation at the neuromuscular junction (James et al., 2019). In addition,
364 dopaminergic circuits associated with reward learning drive release of Ca²⁺ from the
365 endoplasmic reticulum when activated with MB neurons in a backward pairing paradigm *ex vivo*,
366 potentiating MB γ 4 connections with the respective γ 4 MBON (Handler et al., 2019).

367

368 Alterations of MBON activity following learning are likely the product of both synaptic plasticity at
369 the MB-MBON synapses and indirect circuit effects, such as feedforward inhibition (Aso et al.,
370 2014a; Cervantes-Sandoval et al., 2017; Perisse et al., 2016). Polysynaptic inhibitory
371 interactions can convert depression from select MB compartments into potentiation in MBONs
372 following learning. In one established example, reduction of odor-evoked responses in the
373 GABAergic γ 1pedc MBON following aversive conditioning disinhibits the downstream γ 5 β '2a
374 MBON (Owald et al., 2015; Perisse et al., 2016). It is unclear whether this mechanism
375 generalizes to other MB compartments. The present data demonstrates that learning drives
376 potentiation and depression of ACh release across multiple MB compartments, providing a
377 direct mechanism for altering MBON responses. Importantly, by comparing the CS+ and CS-
378 responses to those of untrained odors, we ascribed differences between the CS+ and CS- to
379 potentiation or depression in absolute terms within each compartment. This uncovered an
380 additional layer of spatial regulation of plasticity in the γ 1- γ 3 compartments: a gradient of CS+
381 potentiation to CS- depression following appetitive conditioning, which is elaborated in greater

382 detail below. In addition, it revealed that the IP₃-dependent loss of CS+/CS- contrast was due,
383 at least in large part, to alterations in olfactory adaptation.

384

385 The CS+/CS- relationship changed in a linear gradient down the γ 1- γ 3 compartments following
386 appetitive conditioning. Appetitive conditioning increased CS+ responses in the γ 1
387 compartment, while decreasing the CS- responses in the γ 3 compartment. The γ 2 compartment
388 yielded a mix of these responses. These patterns of plasticity have the net effect of increasing
389 the relative response to the CS+ odor. Since the MBONs postsynaptic to these compartments
390 drive behavioral approach (Aso et al., 2014b), these patterns of plasticity would bias the
391 animal's behavior toward approach of the CS+ if the animal faced both odors simultaneously.
392 Such a situation would occur at the choice point of a T-maze during retrieval in a classical
393 conditioning assay. This further suggests loci where for CS+ and CS- plasticity, which are
394 suggested by behavioral data indicating that temporal/CS- information contribute to behavioral
395 memory (Handler et al., 2019; Konig et al., 2018; Tanimoto et al., 2004; Tully and Quinn, 1985).
396 This is physiologically reflected in plasticity in ACh release to the CS+ and/or CS- across
397 multiple compartments. For instance, the γ 2 and γ 3 compartments exhibited a depression in
398 ACh release to the CS-. Therefore, consequences to the specific timing of odor-evoked
399 responses prior to or after the delivery of the US play a key role in memory formation, with
400 bidirectional plasticity forming within the MB neurons based on timing events, valence of the US,
401 and local dopamine signaling (Handler et al., 2019; Konig et al., 2018; Tanimoto et al., 2004;
402 Yamagata et al., 2016).

403

404 MBONs innervating the γ lobe drive approach/avoidance behavior when stimulated (Aso et al.,
405 2014b). Despite the approach-promoting valence of the $\gamma 2\alpha'1$ and $\gamma 3/\gamma 3\beta'1$ MBONs, only the
406 $\gamma 3/\gamma 3\beta'1$ produced a loss-of-function phenotype in appetitive conditioning. This suggests that
407 either the $\gamma 2\alpha'1$ MBONs are uninvolved in appetitive learning (despite exhibiting learning-related
408 plasticity), or that redundancy and/or different weighting across approach-promoting MBONs,
409 renders the system resilient to silencing some of them. Blocking synaptic output of $\gamma 3/\gamma 3\beta'1$
410 reduced appetitive conditioning performance, suggesting that these neurons play a particularly
411 important role in appetitive learning.

412

413 Overall, plasticity between MB neurons and MBONs may guide behavior through biasing
414 network activation to alter action selection in a probabilistic manner. Appetitive conditioning
415 drives compartmentalized, presynaptic plasticity in MB neurons that correlates with postsynaptic
416 changes in MBONs that guide learned behaviors. Prior studies documented only depression at
417 these synapses at short time points following conditioning (Hige et al., 2015a; Zhang and
418 Roman, 2013; Zhang et al., 2019). Here we observed both potentiation and depression in ACh
419 release in the MB, suggesting that bidirectional presynaptic plasticity modulates learned
420 behaviors. These bidirectional changes likely integrate with plasticity at downstream circuit
421 nodes that also undergo learning-induced plasticity to produce network-level alterations in odor
422 responses across the olfactory pathway following salient events. Thus, plasticity in ACh release
423 from MB neurons function to modulate responsivity to olfactory stimuli features across graded
424 plasticity maps down the mushroom body axons.

425

426 **Materials and Methods**

427 **Fly Strains.** Flies were fed and maintained on a standard cornmeal agar food mixture on a
428 12:12 light:dark cycle. The 238Y-Gal4 driver was selected for expression intensity in MB
429 neurons (Louis et al., 2018). MBON drivers were selected from the FlyLight and split-Gal4
430 collections (R12G04, MB077b, and MB083c) (Jenett et al., 2012; Pfeiffer et al., 2010). The
431 $\gamma 5\beta'2a$ LexA MBON driver was generated by Krystyna Keleman (Zhao et al., 2018). RNAi
432 lines were obtained from the VDRC (Cac: 101478) (Dietzl et al., 2007) and TRiP collections
433 ($IP_3R/itpr$: 25937) (Perkins et al., 2015) and crossed into flies expressing R13F02-Gal4 and tub-
434 Gal80^{ts} (McGuire et al., 2003). Final experimental genotypes were: Cac ($w; UAS-GRAB-$
435 $ACh/UAS-Cac-RNAi; R13F02-Gal4/UAS-tub-Gal80^{ts}$) and IP_3R ($w, UAS-GRAB-ACh/UAS-tub-$
436 $Gal80^{ts}; R13F02-Gal4; UAS-IP3R-RNAi$), compared to genetic controls ($w; UAS-GRAB-$
437 $ACh/+; R13F02-Gal4/UAS-tub- Gal80^{ts}$).

438 **Fly preparation for *in vivo* Ca²⁺ imaging.** Flies were briefly anesthetized, placed in a
439 polycarbonate imaging chamber, and fixed with myristic acid (Sigma-Aldrich). The proboscis
440 was fixed in the retracted position, except for appetitive conditioning experiments (as noted
441 below). A cuticle window was opened, and the fat and tracheal air sacs were carefully removed
442 to allow optical access to the brain. The top of the chamber was filled with saline solution (103
443 mM NaCl, 3mM MBI, 5mM HEPES, 1.5 mM CaCl₂, 4 mM MgCl₂·6H₂O, 26 mM NaHCO₃, 1 mM
444 NaH₂PO₄·H₂O, 10 mM trehalose, 7 mM sucrose, and 10 mM glucose), which was perfused
445 over the dorsal head/brain at 2 mL/min via a peristaltic pump.

446 ***In vivo* imaging.** GRAB-ACh (Jing et al., 2019; Jing et al., 2018; Zhang et al., 2019) was driven
447 in the MB neurons, using the 238Y driver. Within the MB neurons, ROIs were drawn around
448 five γ lobe compartments ($\gamma 1-5$) within a single imaging plane for appetitive, and ($\gamma 2-5$) for
449 aversive. Imaging was performed with a Leica TCS SP8 confocal microscope utilizing
450 appropriate laser lines and emission filter settings. Odors were delivered with an airstream for
451 1s (60mL/min flow rate) by directing the air flow with solenoid valves between an empty vial (air)

452 to another containing 1 μ L odorant spotted on filter paper. Odor-evoked responses were
453 calculated as the baseline normalized change in fluorescence ($\Delta F/F$), using the maximum $\Delta F/F$
454 within a 4-s after odor delivery. The ratio of the post/pre responses were calculated as the
455 maximum $\Delta F/F$ in an 8-s response window after odor delivery. In experiments with RNAi, flies
456 expressing GRAB-ACh, a UAS-RNAi line, and tub-Gal80^{ts} were constructed; flies were raised at
457 18°C until eclosion, flies were transferred to 32°C 4-10 days prior to the experiment.
458 Experiments were carried out at room temperature (23°C) for ACh imaging/conditioning. For
459 Ca²⁺ imaging experiments, GCaMP6f was expressed in the MBONs using the R12G04
460 (γ 1pedc), MB077b (γ 2 α '1), MB083c (γ 3) and VT014702 (γ 5 β '2) Gal4 drivers. Experiments were
461 carried out same as ACh imaging, except presenting a 3s odor delivery.

462 **Appetitive conditioning and imaging.** Appetitive conditioning was carried out as previously
463 described (Louis et al., 2018). One odor (the CS+) was presented in conjunction with a paired
464 sucrose (1M, containing green food coloring) unconditioned stimulus (US), and a second odor
465 (the CS-) was presented 30-s later. Both the CS+ and CS- odors were presented during
466 conditioning experiments. In odor-only control cohorts, the sucrose US was omitted. During
467 training, each odor (and the US) was presented continuously for 30 s for Ca²⁺ imaging
468 experiments. Six 1-s odor pulses were presented during conditioning over a 30-s period, with a
469 5-s inter-pulse interval, to prevent desensitization of the reporter. Pre/post odor-evoked
470 responses were imaged prior to and after the imaging protocol, using a 3-s (Ca²⁺ imaging) or 1-s
471 (ACh imaging) odor pulse. During odor-evoked response imaging, proboscis extension was
472 blocked utilizing a thin metal loop attached to a custom motorized micromanipulator. Flies were
473 starved for a period of 18-24 hrs prior to conditioning. During conditioning, the proboscis was
474 released, and the flies were presented sucrose through a metal pipette fed by a syringe pump
475 controlled via a micro-controller (Arduino). To assess feeding, flies were monitored using a

476 digital microscope (Vividia); sucrose ingestion was visually confirmed by the presence of green
477 food coloring in the abdomen.

478 **Aversive conditioning and imaging.** Flies were mounted in an aversive conditioning chamber
479 such that the brain could be imaged while odors were delivered to the antennae and electric
480 shocks delivered to the legs via a shock grid below the fly. Conditioning was carried out by
481 pairing a CS+ odor with electric shocks as follows: 6x 1-s odor pulses, with a 5-s inter-pulse
482 interval, paired with 6x 90-V electric shocks, followed 30s later by presentation of 6x 1-s pulses
483 of the CS- odor with 5s inter-pulse interval. Pre- and post-conditioning odor-evoked responses
484 were imaged using a 1-s odor pulse. In each animal, either the CS+ or CS- odor was tested
485 pre- and post-conditioning.

486 **Behavioral appetitive conditioning.** Adult flies, 2-5 day old, were trained under dim red
487 light at 75% relative humidity. Appetitive conditioning experiments were performed in animals
488 starved 16-20 h. Groups of ~60 flies were exposed for 2 min to an odor (the CS-), followed by
489 30 s of air and 2 min of another odor, the (the CS+), paired with a 1M sucrose solution dried on
490 filter paper, at 32°C for *Shibire*^{ts} blockade. The odor pairs were ethyl butyrate and isoamyl
491 acetate, adjusted so that naive flies equally avoided the two odors (0.05 – 0.1%). Memory was
492 tested by inserting the trained flies into a T-maze, in which they chose between an arm
493 containing the CS+ odor and an arm containing the CS- odor. Flies were allowed to distribute
494 for a 2 min choice period. The Performance Index (P.I.), calculated as (flies in the CS- arm)-
495 (flies in the CS+ arm)/(total flies in both arms).

496 **Immunohistochemistry.** 5-7 days old adult flies were dissected in 1% paraformaldehyde in S2
497 medium, and processed according to a published protocol (Jenett et al., 2012). Brains and
498 were incubated with the primary antibodies for 3 hours at room temperature and with the
499 secondary antibodies for 4 days at 4°C. Incubations were performed in blocking serum (3%

500 normal goat serum). Labeled brains were mounted in Vectashield media. Antibodies used were
501 rabbit anti-GFP (1:1000, Invitrogen), mouse anti-brp (nc82) (1:50, DSHB), mouse anti-
502 neuroglian (1:50, DSHB), goat anti-rabbit IgG and goat anti-mouse IgG (1:800, Alexa 488 or
503 Alexa 633 respectively, Invitrogen). Images were obtained using Leica TCS SP8 confocal
504 microscope.

505 **Quantification and Statistical Analysis.** Data were compared with ANOVA/Sidak
506 (parametric) or Kruskal-Wallis/Bonferroni (nonparametric) tests. Box plots show graph the
507 median as a line, the 1st and 3rd quartile enclosed in the box, and whiskers extending from the
508 10th to the 90th percentile.

509

510 **Acknowledgments**

511 The authors thank Krystyna Keleman for fly stocks, and Brock Grill for helpful discussions.
512 Stocks obtained from the Bloomington Drosophila Stock Center (NIH P40OD018537) were used
513 in this study. We thank Yuexuan Li for the help in the development of the GRAB-ACh sensor.
514 Research support was provided by NIH R00MH092294, R01 NS097237, the Whitehall
515 Foundation (S.M.T.), NIH R35NS097224 (R.L.D.), the Beijing Municipal Science & Technology
516 Commission Z181100001318002 (Y.L.), the Beijing Brain Initiative of Beijing Municipal Science
517 & Technology Commission Z181100001518004 (Y.L.), Guangdong Grant “Key Technologies for
518 Treatment of Brain Disorders” 2018B030332001 (Y.L.), the General Program of National Natural
519 Science Foundation of China projects 31671118, 31871087, and 31925017 (Y.L.), the NIH
520 BRAIN Initiative NS103558 (Y.L.), grants from the Peking-Tsinghua Center for Life Sciences
521 (Y.L.) and the State Key Laboratory of Membrane Biology at Peking University School of Life
522 Sciences (Y. L.).

523

524 **Competing Interests**

525 The authors declare no competing financial interests.

526

527 **References**

528

529 Aso, Y., Hattori, D., Yu, Y., Johnston, R.M., Iyer, N.A., Ngo, T.T., Dionne, H., Abbott, L., Axel,
530 R., Tanimoto, H., and Rubin, G.M. (2014a). The neuronal architecture of the mushroom body
531 provides a logic for associative learning. *Elife* 3.

532 Aso, Y., Sitaraman, D., Ichinose, T., Kaun, K.R., Vogt, K., Belliard-Guerin, G., Placais, P.Y.,
533 Robie, A.A., Yamagata, N., Schnaitmann, C., *et al.* (2014b). Mushroom body output neurons
534 encode valence and guide memory-based action selection in *Drosophila*. *Elife* 3.

535 Barnstedt, O., Oswald, D., Felsenberg, J., Brain, R., Moszynski, J.P., Talbot, C.B., Perrat, P.N.,
536 and Waddell, S. (2016). Memory-Relevant Mushroom Body Output Synapses Are Cholinergic.
537 *Neuron* 89, 1237-1247.

538 Berry, J.A., Phan, A., and Davis, R.L. (2018). Dopamine Neurons Mediate Learning and
539 Forgetting through Bidirectional Modulation of a Memory Trace. *Cell Rep* 25, 651-662 e655.

540 Boto, T., Louis, T., Jindachomthong, K., Jalink, K., and Tomchik, S.M. (2014). Dopaminergic
541 Modulation of cAMP Drives Nonlinear Plasticity across the *Drosophila* Mushroom Body Lobes.
542 *Curr Biol* 24, 822-831.

543 Boto, T., Stahl, A., Zhang, X., Louis, T., and Tomchik, S.M. (2019). Independent Contributions
544 of Discrete Dopaminergic Circuits to Cellular Plasticity, Memory Strength, and Valence in
545 *Drosophila*. *Cell Rep* 27, 2014-2021 e2012.

546 Cervantes-Sandoval, I., Phan, A., Chakraborty, M., and Davis, R.L. (2017). Reciprocal
547 synapses between mushroom body and dopamine neurons form a positive feedback loop
548 required for learning. *Elife* 6.

549 Cohn, R., Morantte, I., and Ruta, V. (2015). Coordinated and Compartmentalized
550 Neuromodulation Shapes Sensory Processing in *Drosophila*. *Cell* 163, 1742-1755.

551 Crittenden, J.R., Skoulakis, E.M., Han, K.A., Kalderon, D., and Davis, R.L. (1998). Tripartite
552 mushroom body architecture revealed by antigenic markers. *Learn Mem* 5, 38-51.

553 Dietzl, G., Chen, D., Schnorrer, F., Su, K.C., Barinova, Y., Fellner, M., Gasser, B., Kinsey, K.,
554 Opel, S., Scheiblauer, S., *et al.* (2007). A genome-wide transgenic RNAi library for conditional
555 gene inactivation in *Drosophila*. *Nature* 448, 151-156.

556 Frank, C.A., Kennedy, M.J., Goold, C.P., Marek, K.W., and Davis, G.W. (2006). Mechanisms
557 underlying the rapid induction and sustained expression of synaptic homeostasis. *Neuron* 52,
558 663-677.

559 Gervasi, N., Tchenio, P., and Preat, T. (2010). PKA dynamics in a *Drosophila* learning center:
560 coincidence detection by rutabaga adenylyl cyclase and spatial regulation by *dunce*
561 phosphodiesterase. *Neuron* 65, 516-529.

562 Gratz, S.J., Goel, P., Bruckner, J.J., Hernandez, R.X., Khateeb, K., Macleod, G.T., Dickman, D.,
563 and O'Connor-Giles, K.M. (2019). Endogenous Tagging Reveals Differential Regulation of
564 Ca(2+) Channels at Single Active Zones during Presynaptic Homeostatic Potentiation and
565 Depression. *J Neurosci* 39, 2416-2429.

566 Handler, A., Graham, T.G.W., Cohn, R., Morantte, I., Siliciano, A.F., Zeng, J., Li, Y., and Ruta,
567 V. (2019). Distinct Dopamine Receptor Pathways Underlie the Temporal Sensitivity of
568 Associative Learning. *Cell* 178, 60-75 e19.

569 Hendricks, M., Ha, H., Maffey, N., and Zhang, Y. (2012). Compartmentalized calcium dynamics
570 in a *C. elegans* interneuron encode head movement. *Nature* 487, 99-103.
571 Hige, T., Aso, Y., Modi, M.N., Rubin, G.M., and Turner, G.C. (2015a). Heterosynaptic Plasticity
572 Underlies Aversive Olfactory Learning in *Drosophila*. *Neuron* 88, 985-998.
573 Hige, T., Aso, Y., Rubin, G.M., and Turner, G.C. (2015b). Plasticity-driven individualization of
574 olfactory coding in mushroom body output neurons. *Nature* 526, 258-262.
575 Ichinose, T., Aso, Y., Yamagata, N., Abe, A., Rubin, G.M., and Tanimoto, H. (2015). Reward
576 signal in a recurrent circuit drives appetitive long-term memory formation. *Elife* 4, e10719.
577 Inchauspe, C.G., Martini, F.J., Forsythe, I.D., and Uchitel, O.D. (2004). Functional
578 compensation of P/Q by N-type channels blocks short-term plasticity at the calyx of Held
579 presynaptic terminal. *J Neurosci* 24, 10379-10383.
580 Ishikawa, T., Kaneko, M., Shin, H.S., and Takahashi, T. (2005). Presynaptic N-type and P/Q-
581 type Ca²⁺ channels mediating synaptic transmission at the calyx of Held of mice. *J Physiol* 568,
582 199-209.
583 James, T.D., Zwiefelhofer, D.J., and Frank, C.A. (2019). Maintenance of homeostatic plasticity
584 at the *Drosophila* neuromuscular synapse requires continuous IP₃-directed signaling. *Elife* 8.
585 Jenett, A., Rubin, G.M., Ngo, T.T., Shepherd, D., Murphy, C., Dionne, H., Pfeiffer, B.D.,
586 Cavallaro, A., Hall, D., Jeter, J., *et al.* (2012). A GAL4-driver line resource for *Drosophila*
587 neurobiology. *Cell Rep* 2, 991-1001.
588 Jing, M., Li, Y., Zeng, J., Huang, P., Skirzewski, M., Kljakic, O., Peng, W., Qian, T., Tan, K., and
589 Wu, R. (2019). An optimized acetylcholine sensor for monitoring in vivo cholinergic activity.
590 bioRxiv, 861690.
591 Jing, M., Zhang, P., Wang, G., Feng, J., Mesik, L., Zeng, J., Jiang, H., Wang, S., Looby, J.C.,
592 Guagliardo, N.A., *et al.* (2018). A genetically encoded fluorescent acetylcholine indicator for in
593 vitro and in vivo studies. *Nat Biotechnol* 36, 726-737.
594 Kim, Y.C., Lee, H.G., and Han, K.A. (2007). D1 dopamine receptor dDA1 is required in the
595 mushroom body neurons for aversive and appetitive learning in *Drosophila*. *J Neurosci* 27,
596 7640-7647.
597 Konig, C., Khalili, A., Ganesan, M., Nishu, A.P., Garza, A.P., Niewalda, T., Gerber, B., Aso, Y.,
598 and Yarali, A. (2018). Reinforcement signaling of punishment versus relief in fruit flies. *Learn*
599 *Mem* 25, 247-257.
600 Liu, C., Placais, P.Y., Yamagata, N., Pfeiffer, B.D., Aso, Y., Friedrich, A.B., Siwanowicz, I.,
601 Rubin, G.M., Preat, T., and Tanimoto, H. (2012). A subset of dopamine neurons signals reward
602 for odour memory in *Drosophila*. *Nature* 488, 512-516.
603 Louis, T., Stahl, A., Boto, T., and Tomchik, S.M. (2018). Cyclic AMP-dependent plasticity
604 underlies rapid changes in odor coding associated with reward learning. *Proc Natl Acad Sci U S*
605 *A* 115, E448-E457.
606 Lubbert, M., Goral, R.O., Keine, C., Thomas, C., Guerrero-Given, D., Putzke, T., Satterfield, R.,
607 Kamasawa, N., and Young, S.M., Jr. (2019). CaV2.1 alpha1 Subunit Expression Regulates
608 Presynaptic CaV2.1 Abundance and Synaptic Strength at a Central Synapse. *Neuron* 101, 260-
609 273 e266.
610 Mao, Z., and Davis, R.L. (2009). Eight different types of dopaminergic neurons innervate the
611 *Drosophila* mushroom body neuropil: anatomical and physiological heterogeneity. *Front Neural*
612 *Circuits* 3, 5.
613 McGuire, S.E., Le, P.T., and Davis, R.L. (2001). The role of *Drosophila* mushroom body
614 signaling in olfactory memory. *Science* 293, 1330-1333.
615 McGuire, S.E., Le, P.T., Osborn, A.J., Matsumoto, K., and Davis, R.L. (2003). Spatiotemporal
616 rescue of memory dysfunction in *Drosophila*. *Science* 302, 1765-1768.
617 Modi, M.N., Shuai, Y., and Turner, G.C. (2020). The *Drosophila* Mushroom Body: From
618 Architecture to Algorithm in a Learning Circuit. *Annu Rev Neurosci* 43, 465-484.

619 Muller, M., and Davis, G.W. (2012). Transsynaptic control of presynaptic Ca²⁺(+) influx
620 achieves homeostatic potentiation of neurotransmitter release. *Curr Biol* 22, 1102-1108.
621 Nanou, E., Scheuer, T., and Catterall, W.A. (2016). Calcium sensor regulation of the CaV2.1
622 Ca²⁺ channel contributes to long-term potentiation and spatial learning. *Proc Natl Acad Sci U S*
623 *A* 113, 13209-13214.
624 Oswald, D., Felsenberg, J., Talbot, C.B., Das, G., Perisse, E., Huetteroth, W., and Waddell, S.
625 (2015). Activity of defined mushroom body output neurons underlies learned olfactory behavior
626 in *Drosophila*. *Neuron* 86, 417-427.
627 Perisse, E., Oswald, D., Barnstedt, O., Talbot, C.B., Huetteroth, W., and Waddell, S. (2016).
628 Aversive Learning and Appetitive Motivation Toggle Feed-Forward Inhibition in the *Drosophila*
629 Mushroom Body. *Neuron* 90, 1086-1099.
630 Perkins, L.A., Holderbaum, L., Tao, R., Hu, Y., Sopko, R., McCall, K., Yang-Zhou, D., Flockhart,
631 I., Binari, R., Shim, H.S., *et al.* (2015). The Transgenic RNAi Project at Harvard Medical School:
632 Resources and Validation. *Genetics* 201, 843-852.
633 Pfeiffer, B.D., Ngo, T.T., Hibbard, K.L., Murphy, C., Jenett, A., Truman, J.W., and Rubin, G.M.
634 (2010). Refinement of tools for targeted gene expression in *Drosophila*. *Genetics* 186, 735-755.
635 Placais, P.Y., Trannoy, S., Friedrich, A.B., Tanimoto, H., and Preat, T. (2013). Two pairs of
636 mushroom body efferent neurons are required for appetitive long-term memory retrieval in
637 *Drosophila*. *Cell Rep* 5, 769-780.
638 Rowan, M.J., DelCanto, G., Yu, J.J., Kamasawa, N., and Christie, J.M. (2016). Synapse-Level
639 Determination of Action Potential Duration by K(+) Channel Clustering in Axons. *Neuron* 91,
640 370-383.
641 Sayin, S., De Backer, J.F., Siju, K.P., Wosniack, M.E., Lewis, L.P., Frisch, L.M., Gansen, B.,
642 Schlegel, P., Edmondson-Stait, A., Sharifi, N., *et al.* (2019). A Neural Circuit Arbitrates between
643 Persistence and Withdrawal in Hungry *Drosophila*. *Neuron* 104, 544-558 e546.
644 Scaplen, K.M., Talay, M., Fisher, J.D., Cohn, R., Sorkac, A., Aso, Y., Barnea, G., and Kaun,
645 K.R. (2021). Transsynaptic mapping of *Drosophila* mushroom body output neurons. *Elife* 10.
646 Schroll, C., Riemensperger, T., Bucher, D., Ehmer, J., Voller, T., Erbguth, K., Gerber, B.,
647 Hendel, T., Nagel, G., Buchner, E., and Fiala, A. (2006). Light-induced activation of distinct
648 modulatory neurons triggers appetitive or aversive learning in *Drosophila* larvae. *Curr Biol* 16,
649 1741-1747.
650 Schwaerzel, M., Monastirioti, M., Scholz, H., Friggi-Grelin, F., Birman, S., and Heisenberg, M.
651 (2003). Dopamine and octopamine differentiate between aversive and appetitive olfactory
652 memories in *Drosophila*. *J Neurosci* 23, 10495-10502.
653 Sejourne, J., Placais, P.Y., Aso, Y., Siwanowicz, I., Trannoy, S., Thoma, V., Tedjakumala, S.R.,
654 Rubin, G.M., Tchenio, P., Ito, K., *et al.* (2011). Mushroom body efferent neurons responsible for
655 aversive olfactory memory retrieval in *Drosophila*. *Nat Neurosci* 14, 903-910.
656 Takemura, S.Y., Aso, Y., Hige, T., Wong, A., Lu, Z., Xu, C.S., Rivlin, P.K., Hess, H., Zhao, T.,
657 Parag, T., *et al.* (2017). A connectome of a learning and memory center in the adult *Drosophila*
658 brain. *Elife* 6.
659 Tanaka, N.K., Tanimoto, H., and Ito, K. (2008). Neuronal assemblies of the *Drosophila*
660 mushroom body. *J Comp Neurol* 508, 711-755.
661 Tanimoto, H., Heisenberg, M., and Gerber, B. (2004). Experimental psychology: event timing
662 turns punishment to reward. *Nature* 430, 983.
663 Taufiq, A.M., Fujii, S., Yamazaki, Y., Sasaki, H., Kaneko, K., Li, J., Kato, H., and Mikoshiba, K.
664 (2005). Involvement of IP3 receptors in LTP and LTD induction in guinea pig hippocampal CA1
665 neurons. *Learn Mem* 12, 594-600.
666 Tomchik, S.M., and Davis, R.L. (2009). Dynamics of learning-related cAMP signaling and
667 stimulus integration in the *Drosophila* olfactory pathway. *Neuron* 64, 510-521.
668 Tully, T., and Quinn, W.G. (1985). Classical conditioning and retention in normal and mutant
669 *Drosophila melanogaster*. *J Comp Physiol A* 157, 263-277.

670 Xu, C.S., Januszewski, M., Lu, Z., Takemura, S.-y., Hayworth, K., Huang, G., Shinomiya, K.,
671 Maitin-Shepard, J., Ackerman, D., and Berg, S. (2020). A Connectome of the Adult *Drosophila*
672 Central Brain. *bioRxiv*.
673 Yamagata, N., Hiroi, M., Kondo, S., Abe, A., and Tanimoto, H. (2016). Suppression of
674 Dopamine Neurons Mediates Reward. *PLoS Biol* 14, e1002586.
675 Yamagata, N., Ichinose, T., Aso, Y., Placais, P.Y., Friedrich, A.B., Sima, R.J., Preat, T., Rubin,
676 G.M., and Tanimoto, H. (2015). Distinct dopamine neurons mediate reward signals for short-
677 and long-term memories. *Proc Natl Acad Sci U S A* 112, 578-583.
678 Zamponi, G.W., and Currie, K.P. (2013). Regulation of Ca(V)₂ calcium channels by G protein
679 coupled receptors. *Biochim Biophys Acta* 1828, 1629-1643.
680 Zars, T., Fischer, M., Schulz, R., and Heisenberg, M. (2000). Localization of a short-term
681 memory in *Drosophila*. *Science* 288, 672-675.
682 Zhang, S., and Roman, G. (2013). Presynaptic inhibition of gamma lobe neurons is required for
683 olfactory learning in *Drosophila*. *Curr Biol* 23, 2519-2527.
684 Zhang, X., Noyes, N.C., Zeng, J., Li, Y., and Davis, R.L. (2019). Aversive Training Induces Both
685 Presynaptic and Postsynaptic Suppression in *Drosophila*. *J Neurosci* 39, 9164-9172.
686 Zhao, X., Lenek, D., Dag, U., Dickson, B.J., and Keleman, K. (2018). Persistent activity in a
687 recurrent circuit underlies courtship memory in *Drosophila*. *Elife* 7.
688

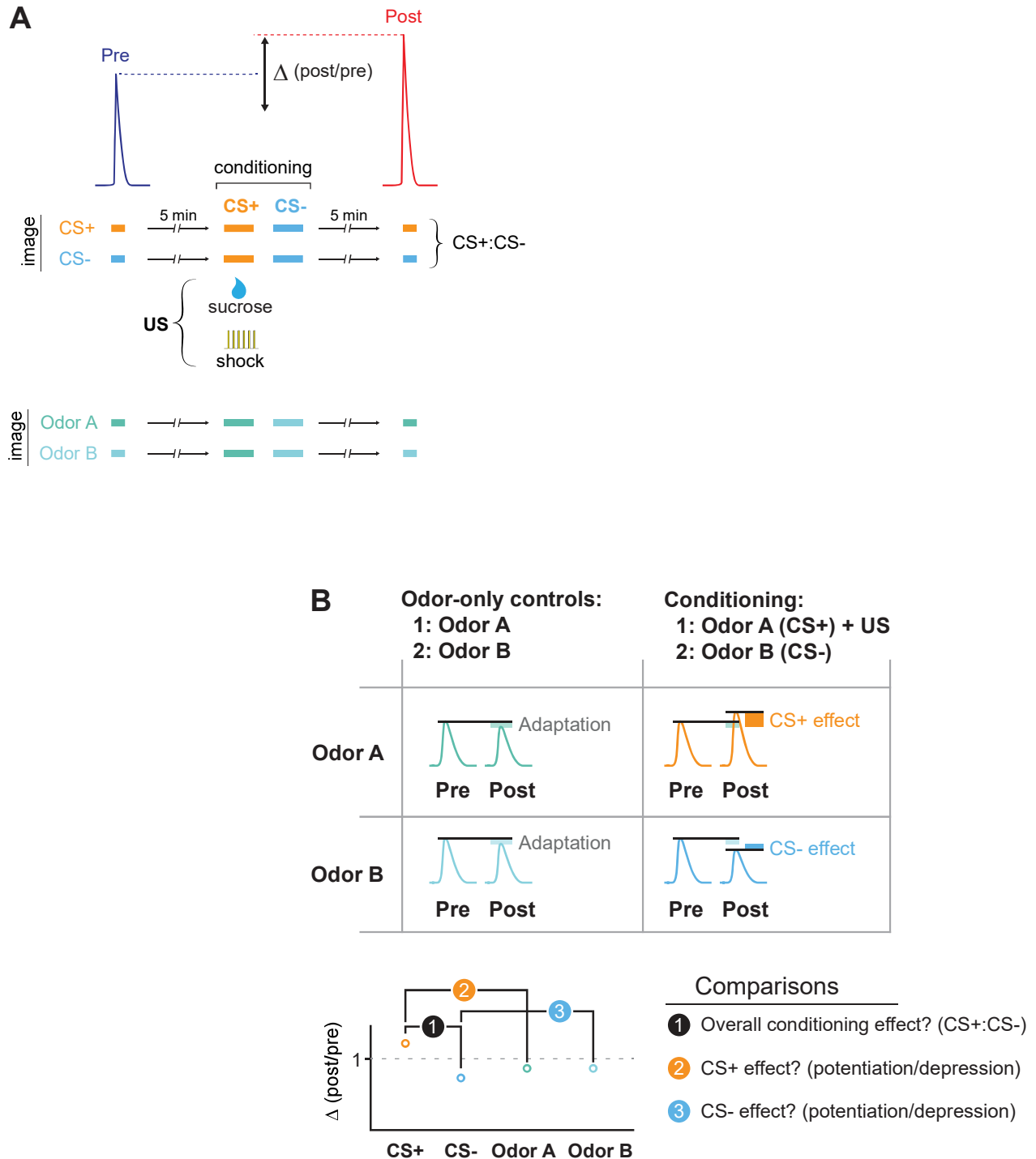


Figure S1, related to Figure 1. The conditioning and imaging assay and data analysis. **(A)** Flies were conditioned by pairing an odor (the CS+) with a US (electric shock or sucrose reward), and a second odor (the CS-) was presented afterward. Odor-evoked GCh or GCaMP responses were imaged in the MB and compared before (Pre) and after (Post) conditioning. Responses were compared to animals in which the same odors were presented, but no US presented (odor-only controls). To examine how conditioning (or odor-only presentation) changed the odor responses, the Δ (post/pre) was calculated for each treatment. **(B)** Two types of comparisons were made across conditions. First, we analyzed the CS+:CS- ratio, which mimics the putative comparison the animal makes when comparing the two odors at the choice point in a T-maze during memory retrieval. Second, we compared the CS+ and CS- to their respective odor-only controls in order to determine whether the responses were potentiated or depressed by conditioning. This comparison normalizes for any olfactory adaptation that is induced by the odor presentation during the training window.

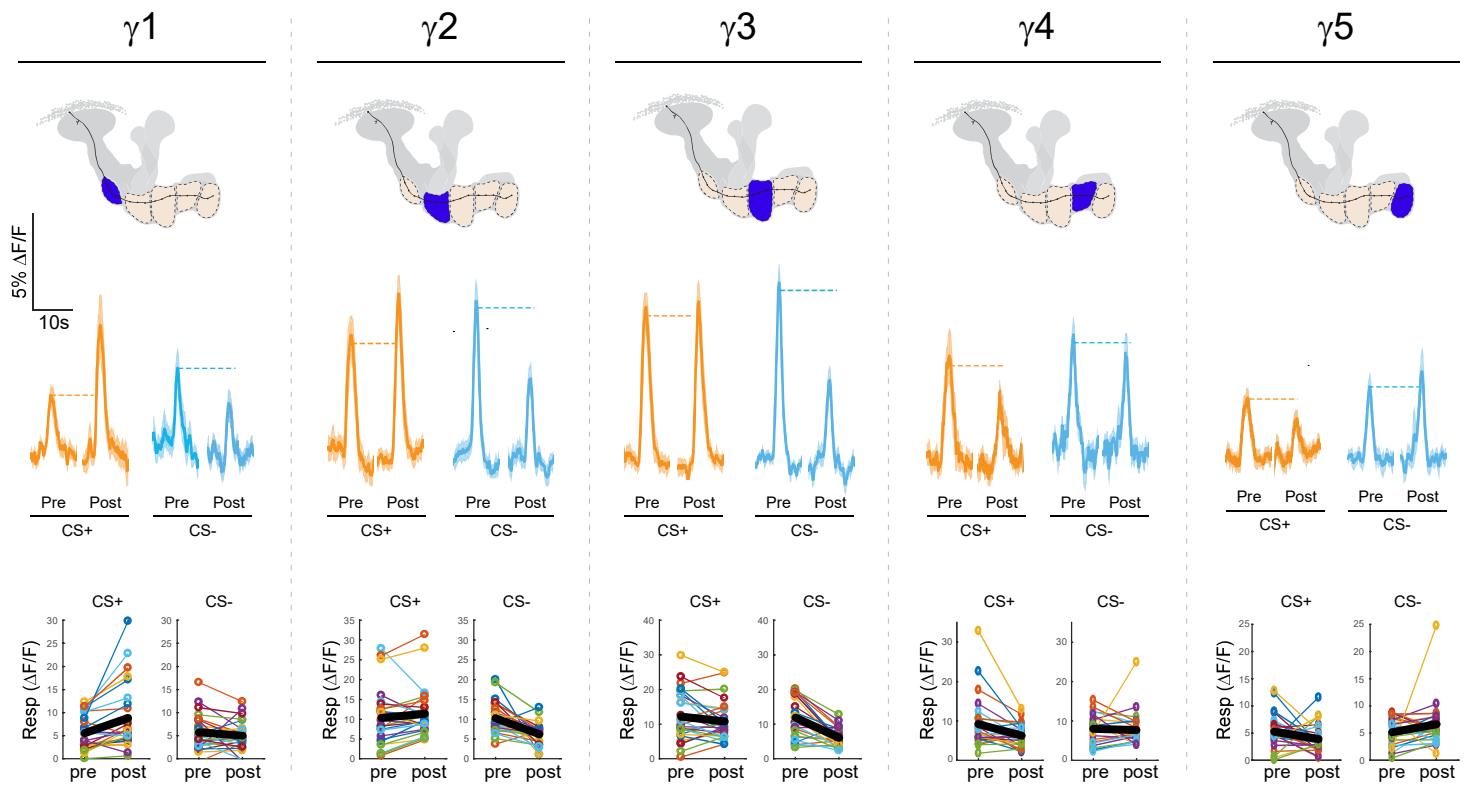


Figure S2, related to Figure 1. Effects of appetitive conditioning on GRAB-ACh responses across the γ lobe compartments. The top row shows diagrams of the location of each compartment within the mushroom body. The second row shows time series traces pre- and post-conditioning for the CS+ (ethyl butyrate [EB]) and CS- (isoamyl acetate [IA]). The third row shows quantification of the peak pre- and post-conditioning responses for each animal (n = 27). The thick black line represents the mean.

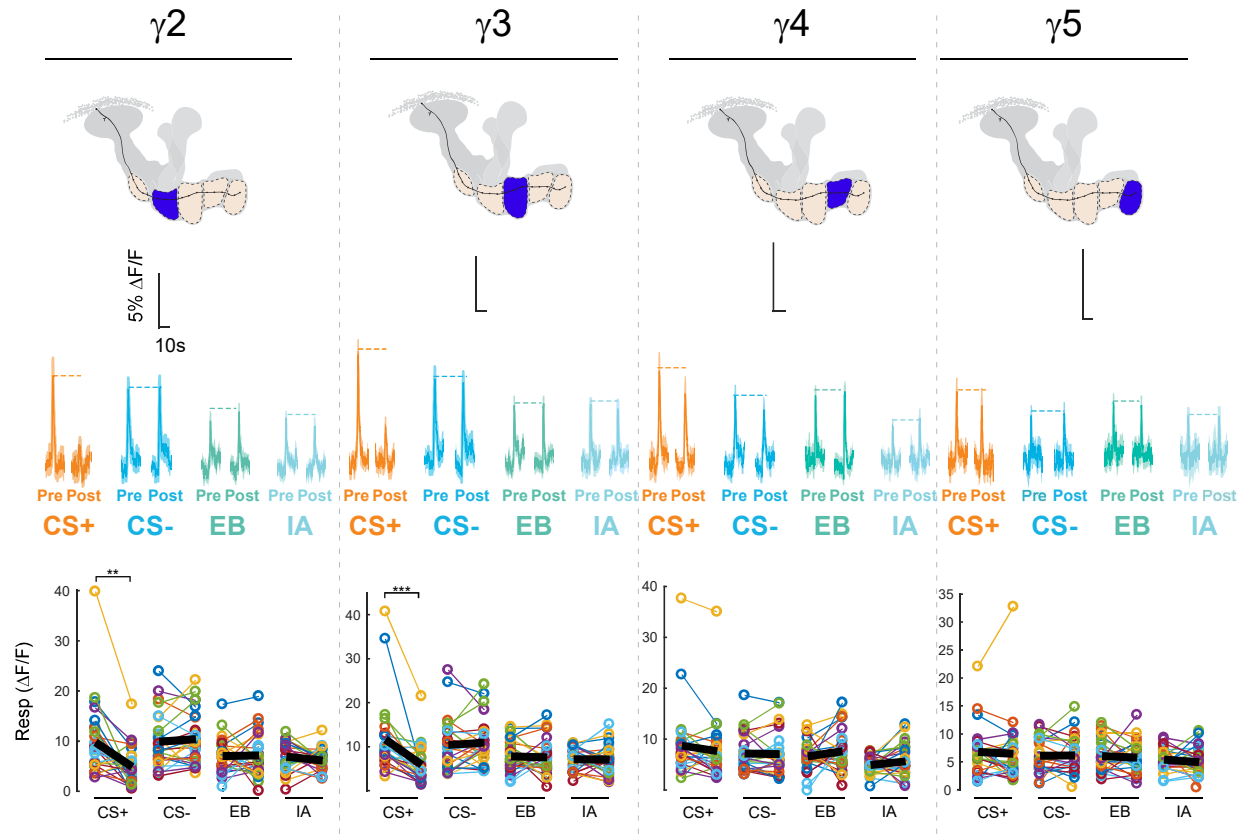


Figure S3, related to Figure 2. Effects of aversive conditioning on GRAB-ACh responses across the γ lobe compartments. The top row shows diagrams of the location of each compartment within the mushroom body. The second row shows time series traces pre- and post-conditioning for the CS+ (ethyl butyrate [EB]) and CS- (isoamyl acetate [IA]) and odor only controls. The third row shows quantification of the peak pre- and post-conditioning responses for each animal ($n = 27$). * $p < 0.05$, ** $p < 0.005$, *** $p < 0.0005$ $n = 12$ (Wilcoxon rank-sum test). The thick black line represents the mean.

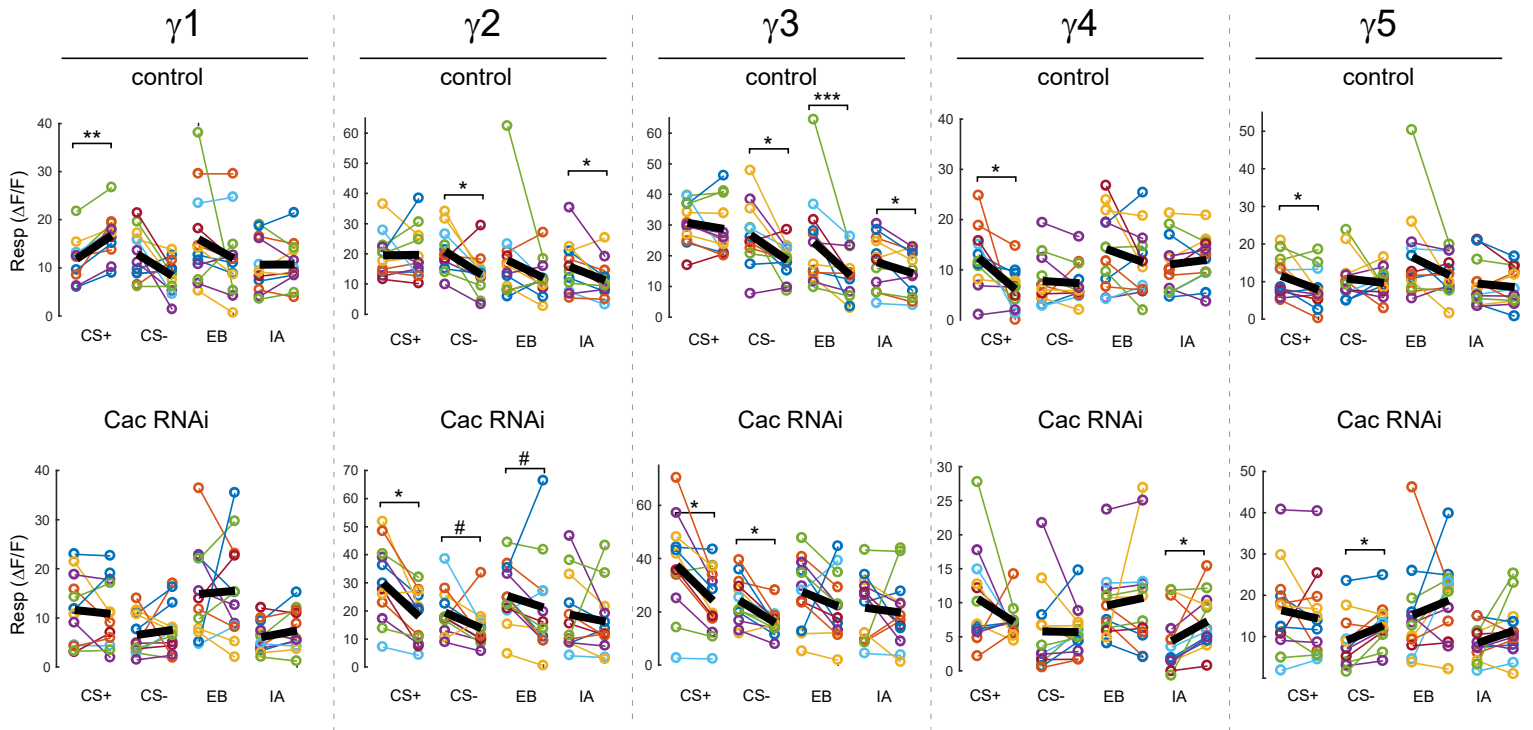


Figure S4, related to Figure 3. Effects of appetitive conditioning on GRAB-ACh responses across the γ lobe compartments using GRAB-ACh with control and cacophony knockdown flies. The top row shows time series traces pre- and post-conditioning for the CS+ (ethyl butyrate [EB]) and CS- (isoamyl acetate [IA]) of control flies. The quantification of the peak pre- and post-conditioning responses for each animal ($n = 12$) of control flies. * $p < 0.05$, ** $p < 0.005$, *** $p < 0.0005$, # $p < 0.07$, $n = 12$ (Wilcoxon rank-sum test). The second row shows time series traces pre- and post-conditioning Cac knockdowns.

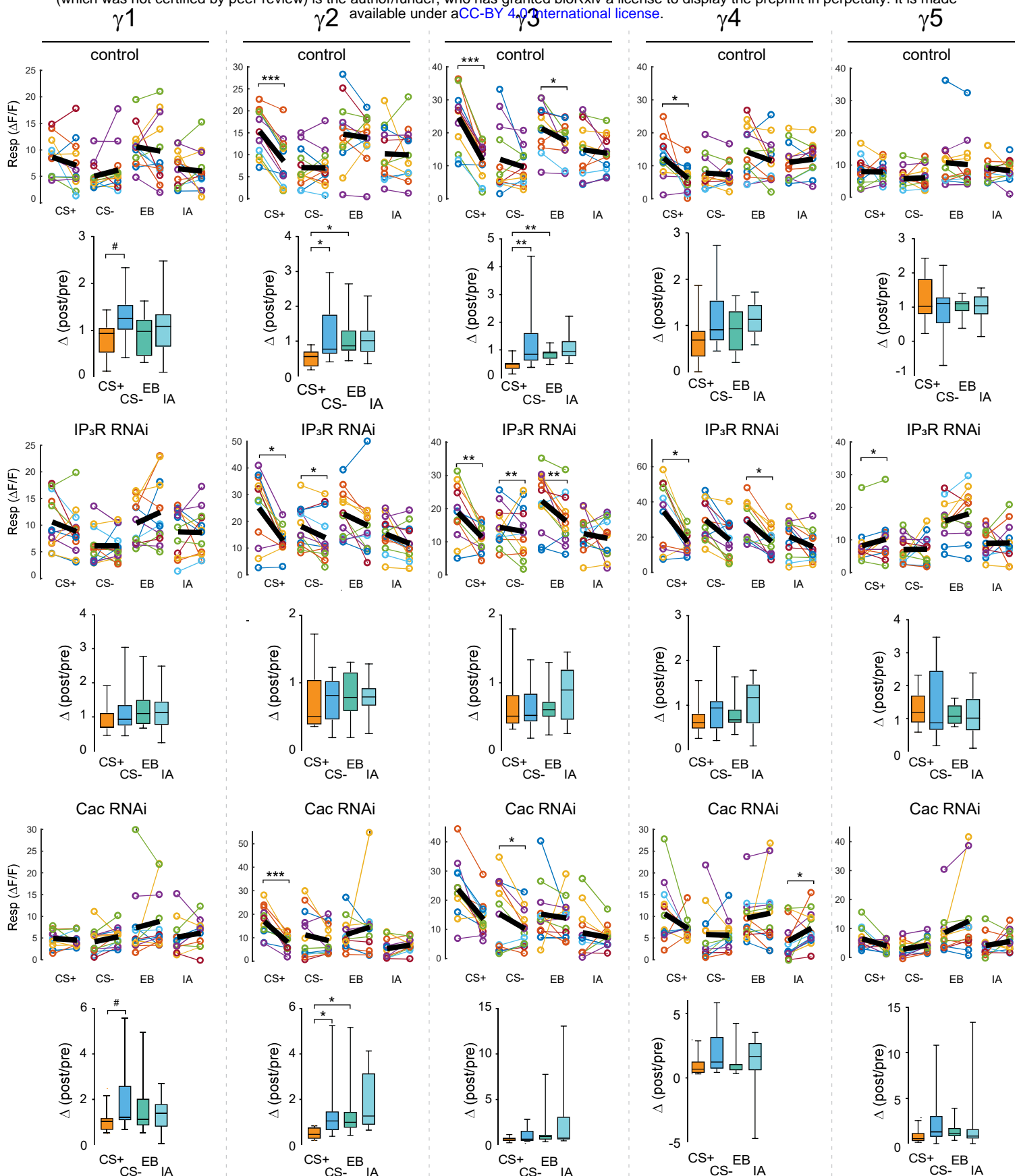


Figure S5, related to Figure 4. Effects of aversive conditioning on GRAB-ACh responses across the γ lobe compartments using GRAB-ACh with control, cacophony and IP₃R knockdown flies. For all genotypes sample sizes, n=12 with statistical analysis (Wilcoxon rank-sum test) *p<0.05, **p<0.005, ***p<0.0005 for time series traces. For comparisons of CS+, CS-, and odor-only control responses (Kruskal-Wallis/Bonferroni) #p<0.03, *p<0.01, **p<0.001, ***p<0.0001. The top row shows time series traces pre- and post-conditioning for the CS+ (ethyl butyrate [EB]) and CS- (isoamyl acetate [IA]) and odor only, and the thick black line represents the mean. The second row shows comparisons of the CS+, CS-, and odor-only controls. The third row shows time series traces pre-post conditioning for IP₃R knockdowns. The fourth row shows comparisons between the four treatments of IP₃R knockdowns. The fifth row shows time series traces pre-post conditioning for Cac knockdowns. The final row shows comparisons between the four treatments of Cac knockdowns.

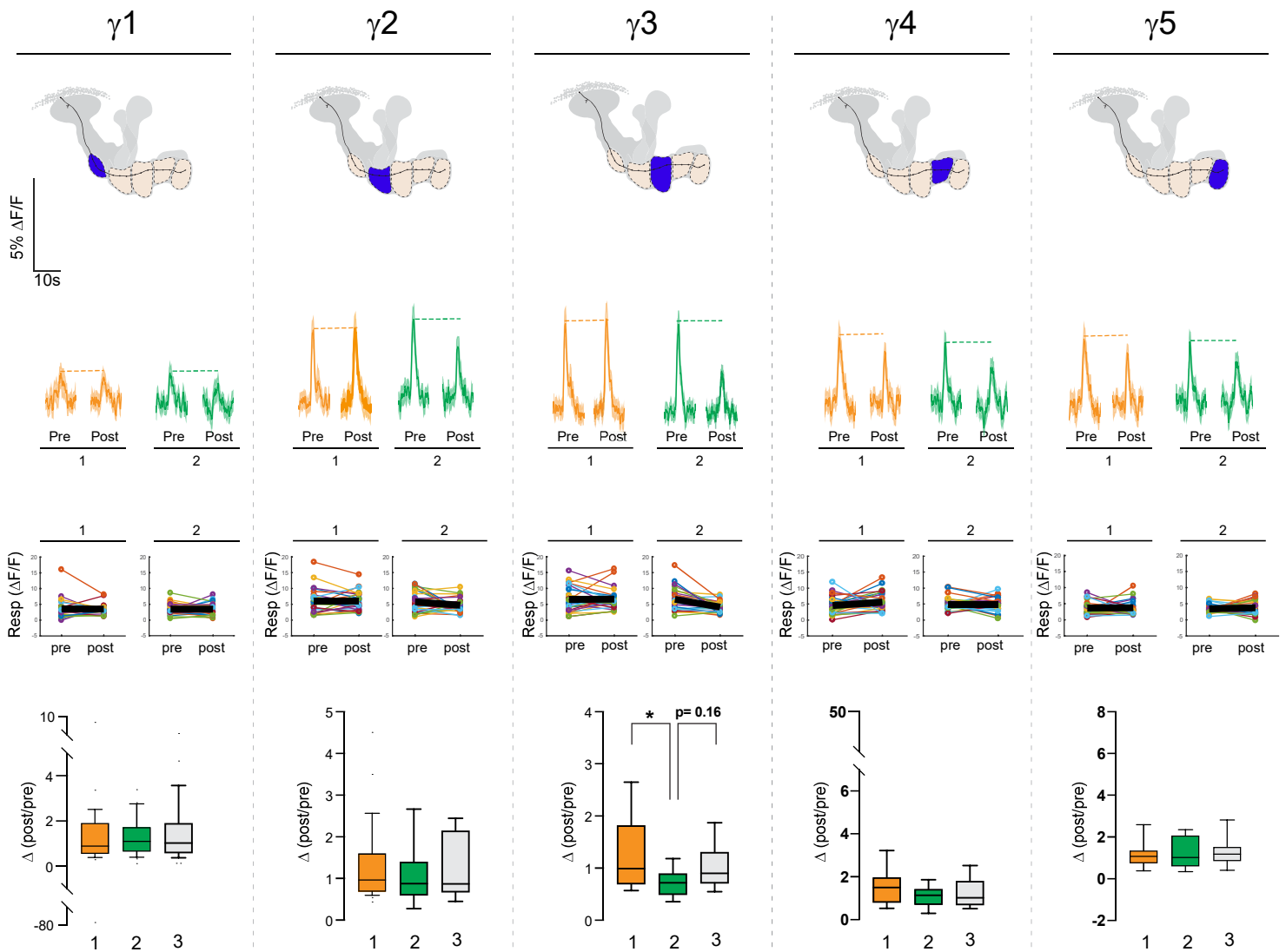


Figure S6, related to Figure 6. Effects of appetitive conditioning on GRAB-ACh responses across the γ lobe in the absence of either CS+ (1) or CS- (2). The top row shows diagrams of the location of each compartment within the mushroom body. The second row shows time series traces pre- and post-conditioning for paired, unpaired, and odor-only conditioning. The third row shows quantification of the peak pre- and post-conditioning responses for each animal ($n = 27$). The thick black line represents the mean. The bottom row shows comparisons of the CS+, CS-, and odor-only controls (EB and IA). * $p < 0.01$, ** $p < 0.001$, *** $p < 0.0001$; $n = 27$ (Kruskal-Wallis/Bonferroni).